High-stress corners
December 2011

PD Cenek, PK Herrington, RJ Henderson, BJH Holland, IR McIver and DK Walton
Opus Central Laboratories

NZ Transport Agency research report 466

ISBN 978-0-478-38088-0 (print)
ISBN 978-0-478-38087-3 (electronic)
ISSN 1173-3756 (print)
ISSN 1173-3764 (electronic)

NZ Transport Agency
Private Bag 6995, Wellington 6141, New Zealand
Telephone 64 4 894 5400; facsimile 64 4 894 6100
research@nzta.govt.nz
www.nzta.govt.nz

Cenek, PD, PK Herrington, RJ Henderson, BJH Holland, IR McIver[1] and DK Walton[2] (2011) High-stress corners. *NZ Transport Agency research report 466.* 58pp.

Opus Central Laboratories, PO Box 30 845, Gracefield, Lower Hutt
[1] Now an employee of GREENBeing
[2] Now an employee of Health Sponsorship Council

Keywords: chip loss, cornering forces, high-stress curves, scuffing

An important note for the reader

The NZ Transport Agency is a Crown entity established under the Land Transport Management Act 2003. The objective of the Agency is to undertake its functions in a way that contributes to an affordable, integrated, safe, responsive and sustainable land transport system. Each year, the NZ Transport Agency funds innovative and relevant research that contributes to this objective.

The views expressed in research reports are the outcomes of the independent research, and should not be regarded as being the opinion or responsibility of the NZ Transport Agency. The material contained in the reports should not be construed in any way as policy adopted by the NZ Transport Agency or indeed any agency of the NZ Government. The reports may, however, be used by NZ Government agencies as a reference in the development of policy.

While research reports are believed to be correct at the time of their preparation, the NZ Transport Agency and agents involved in their preparation and publication do not accept any liability for use of the research. People using the research, whether directly or indirectly, should apply and rely on their own skill and judgement. They should not rely on the contents of the research reports in isolation from other sources of advice and information. If necessary, they should seek appropriate legal or other expert advice.

Acknowledgements

The authors gratefully acknowledge contributions to this research programme by the NZ Transport Agency who supplied data and funded the research described here and the peer-reviewers for their many helpful comments. The specialist input of the following Opus Central Laboratories staff is also recognised:

- G.F.A. Ball for performing the statistical analysis of curve speeds
- R.J. Kean for assisting in the selection of instrumentation for obtaining vehicle heading data
- M.W. McLarin for performing vehicle simulations to quantify peak lateral and vertical tyre forces.

Contents

Executive summary

This report details research carried out during the period 2003–11 by Opus International Consultants, Central Laboratories, Gracefield, Lower Hutt, New Zealand. The original aim of this research was to optimise the performance of chipseal surfacing on high-stress corners by developing a systematic process for categorising the severity of such sites. The intention was that this categorisation process would allow a designer to establish the probability of chip loss on a given section of pavement and so select an appropriate surface to ensure adequate performance.

The research involved three distinct parts as follows:

1 Determination of tyre forces during cornering manoeuvres.

2 Finite element analysis of stresses induced in the bitumen binder by cornering vehicles.

3 Statistical modelling involving the variable labelled 'scabbing' in the NZ Transport Agency's (NZTA) road asset maintenance management (RAMM) database.

These are expanded on below.

Tyre to pavement forces

The first step in the research was to confirm there was a link between chip loss on curves and high stress through determining tyre forces on 13 test road sections where chip loss in the wheel paths was present. This investigation used measured vehicle paths and traffic speeds which were subsequently used as inputs to vehicle simulation software to calculate the individual tyre forces acting on the pavement.

Calculated tyre forces between curves, wheel paths and lanes were compared. Relationships were then formed between the locations of peak tyre forces and the locations of chip loss. The first major result from this research was that the peak lateral force on a corner occurred below the wheels in the outside wheel path. As horizontal stress was thought to be the main cause of chip loss, this finding was worrying as in most cases chip loss has been observed to occur in the inside wheel path.

To form a more accurate picture of the forces causing chip loss, the peak force ratio was derived. This measure was defined as the ratio of the peak lateral force to the peak vertical force averaged for each wheel path. When the distribution of the peak force ratio was examined, it was found to occur predominantly in the inside wheel path of each curve. To further examine if the peak force ratio did in fact have an influence on chip loss, the location of the peak force ratio for each curve investigated was compared to the location of the centre of chip loss. These locations were found to correlate very well, generating an r^2 value of 0.96. This showed although the horizontal component of tyre force acting on the pavement was a large factor in chip loss, the combination of a high lateral force with a low vertical force was an even stronger factor.

Another interesting result of the initial research was that chip loss appeared to be predominantly related to the inside lane of left-hand turns. However, the most significant result was that although a link between chip loss on curves and high stress was established, the converse was not, ie high pavement stress from cornering did not always result in chip loss.

Finite element analysis

The investigation of the physical mechanism of chip loss involved finite element analysis of pavement sections subjected to stresses induced by cornering light vehicles and trucks. This was done to determine if the forces applied were sufficient to exceed the failure stress in bitumen.

The finite element analysis was performed on two separate chipseal samples, one with grade 2 chip and the other with grade 4. The loadings applied to the chipseal geometries were based on a truck taking a 50m radius curve at sufficient speed to generate 0.25g of lateral acceleration, relating to a speed of approximately 40km/h. This model was then extrapolated to examine 0.4g and 0.5g lateral accelerations. By comparison, curves are designed to produce a lateral acceleration in the range of zero to 0.1g at the design cornering speed.

It was found the stresses induced by a truck cornering under the above conditions could be sufficient to cause localised failures of the bitumen binder. However, the failed area was considered to be of insufficient size to cause chips to strip from the seal.

Statistical analysis

To obtain a more accurate view of factors influencing chip loss, statistical correlations were performed using a chip loss variable (scabbing) with a variety of variables obtained from NZTA's RAMM database. The results of these correlations found horizontal curvature was only a very slight predictor of chip loss, raising some fundamental questions about the conventional predictors of chip loss and leading to a change of focus in the research. This change of focus put more emphasis on finding the true predictors of chip loss and investigating more closely the underlying mechanism, although research continued on the original work of modelling tyre forces.

The correlations were performed between 33 traffic, curve geometry and seal-related variables contained in the RAMM database and the chip loss variable scabbing. Scabbing is used in RAMM to denote the area of a carriageway where the seal has lost more than 10% of the sealing chip. Generally, the correlation values were all very low ($r < 0.2$) apart from pavement source ($r=0.37$) and the NZTA's administration region ($r=0.50$). Importantly, the correlation study did not find a particular seal type was more susceptible to chip loss than any other.

The study into the predictors of chip loss took the form of further statistical analysis including the development of several logistic regression models attempting to explain chip loss. These models confirmed there were regional differences in the drivers of chip loss.

Conclusions

- If chip loss is observed on curves, it tends to occur where large lateral tyre loading is combined with small vertical tyre loading. This corresponds to the tightest part of the curve in the innermost wheel path.
- It was determined from finite element modelling that even at lateral accelerations five times the level normally expected for properly designed curves, the stresses generated in single coat chipseals were insufficient to cause failure of the binder in large enough areas to cause chip loss.
- The statistical modelling identified that chip loss on curves correlated the strongest with the NZTA administration region. Further investigation using logistic regression modelling suggested that in some regions, traffic, curve geometry and seal-related variables stored in the RAMM database were a

good predictor of chip loss whereas in other regions this was not the case. This suggests there are regional differences in the drivers of chip loss. There is a range of potential reasons for this result which include climate, sealing chip properties and construction practices.

- Taken overall, the research found there were two principal factors influencing chip loss induced by cornering vehicles:
  - bitumen failing from the induced stress
  - packing and embedment of the pavement surface layer aggregate chips.

  Of these two factors, the dominant one is aggregate packing and embedment. Therefore, the research supports previous findings that it is not the seal design but construction practices, notably the use of controlled traffic to bed the sealing chips, which have the greatest influence in mitigating chip loss.

Recommendations

- Attention should be paid to ensuring surface compaction by controlling trafficking in the 48-hour period after chipseal construction to reduce the likelihood of chip loss.
- Where there is a concern over chip loss, consideration should be given to the use of smaller chip sizes to reduce the stress in the bitumen, but this has to be weighed up against the potential for flushing.
- On curves, superelevation (ie camber) helps to counterbalance the lateral acceleration of vehicles thereby reducing the horizontal stresses applied to the chipseal surface. Therefore, there is additional scope for reducing the occurrence of chip loss on tight (ie horizontal radius less than 300m) curves through ensuring the superelevation is at the recommended design level for the curve radius.
- The finite element simulations performed suggest the forces induced by cornering traffic may be insufficient to cause failure in the bitumen binder of well constructed roads in some situations. To confirm this, it is recommended additional finite element simulations are performed for a wide range of vehicle types, curve radii and superelevations, vehicle speeds, tyre inflation pressures and pavement aggregate grades. Such a study would also help to either support or negate the finding that the induced stress in chipseal surfacings decreases with increasing aggregate grade.
- A limited analysis of vehicle speeds around curves with a horizontal radius of curvature ranging from about 30m to 215m resulted in two unexpected findings. The first was that lane roughness has a significant influence on the curve speed. The second was that the 99th percentile curve speed of heavy commercial vehicles was the same as that of passenger cars. Given the significance of these findings for speed management and surfacing design, a more comprehensive investigation of vehicle speed distributions on tight curves should be undertaken to establish robust relationships for estimating different percentile curve speeds as a function of vehicle class.

Abstract

A programme of research was undertaken to better understand chip loss on curves with the aim to improve chipseal design and selection practices. The research involved on-road measurements and computer simulation of tyre forces during cornering manoeuvres; correlation analysis using road surface, road geometry and traffic variables contained in the NZ Transport Agency's RAMM database; and finite element analysis of pavement surface stresses induced by a cornering truck.

The key findings were:

1 There was not a particular chipseal type more prone to chip loss than others.

2 It was determined from the finite element modelling that even at lateral accelerations five times the level normally expected for properly designed curves, the stresses generated in single coat chipseals were insufficient to cause failure of the binder in large enough areas to cause chip loss.

3 The RAMM variable that correlated the strongest with chip loss on curves was the NZ Transport Agency administration region suggesting climate, sealing properties or construction practices as being the main drivers not lateral acceleration.

These findings support previous research that it is not seal design but construction practices, notably the use of controlled traffic to bed the sealing chips, which have the largest influence on mitigating chip loss.

1 Introduction

The original aim of this research was to optimise the performance of chipseal surfacing on high-stress corners by developing a systematic process for categorising the severity of such sites. This would allow a designer to find the probability of chip loss on a given section of pavement and to select an appropriate surface to ensure adequate performance.

The first step in the research was to confirm there was a link between chip loss on curves and high stress through determining tyre forces on 13 test road sections where chip loss in the wheel paths was present. While this was found to be true, the converse was not found, ie that there was a link between high stress and chip loss. Accordingly, a theoretical study involving a 2D finite element (FE) model of a representative chipseal was performed to determine if the levels of stress applied from the wheel loading that typically occurred during tight cornering would be sufficiently large to cause the bond between the sealing chip and bitumen to fail. It was found the stresses were high in small areas of the bitumen in the chipseal. However, these stresses and areas were considered an unlikely cause of the bitumen failing and causing chips to be stripped from the seal.

To obtain a more accurate view of factors influencing chip loss, an analysis was carried out to investigate the degree of correlation between the variable labelled 'scabbing' in the NZ Transport Agency's (NZTA) road asset maintenance management (RAMM) database, which is used to denote the area of a carriageway where the seal has lost more than 10% of the sealing chip and other road geometry, surfacing and traffic related variables also stored in the RAMM database. The results of this correlation study confirmed horizontal curvature was a poor predictor of chip loss. Further it was found the network area gave the highest correlation with chip loss as described by the scabbing variable, although the correlation value was still low.

The study into the predictors of chip loss took the form of further statistical analysis including the development of several logistic regression models attempting to explain chip loss. The results of the statistical analysis also proved useful in the testing of several hypotheses relating to chip loss.

This report summarises the principal findings arising from the analysis of wheel loading during cornering and statistical modelling of chipseal loss undertaken during the period 2003–11. The report has been structured as follows.

- Chapter 1 overviews the research undertaken.
- Chapter 2 considers the relationship between lateral and vertical tyre/pavement forces generated and observed chip loss for a small passenger car.
- Chapter 3 investigates various vehicle type/cornering speed scenarios to determine if the resulting tyre forces are sufficient to cause failure stresses in bitumen. The condition of low-speed tyre scrubbing is also analysed.
- Chapter 4 presents the results of the statistical modelling of chip loss using data from NZTA's RAMM database.
- Chapter 5 discusses the influence of construction practices on the occurrence of chip loss.
- Chapter 6 provides a summary of the main discussion points arising from the research.
- Chapter 7 contains the main conclusions and associated recommendations.

- Procedures for calculating lateral accelerations from RAMM geometry data, simulation derived estimates of tyre forces at each of the 13 test sites for three different types of vehicle, and an analysis of actual curve speed distributions are presented in appendices A, B and C respectively.
- Appendix D is a glossary of terms and variables used in this report.

2 Tyre forces during cornering

It is known that chip loss can be caused by traffic-induced horizontal stresses acting on the chipseal surface. These stresses will vary in magnitude and direction from tyre to tyre and from curve to curve depending on a wide range of variables. The first stage of the research involved quantifying tyre forces during typical cornering manoeuvres and relating the location and directional composition of these forces to observed chip loss.

Several methods exist for measuring or simulating the lateral forces acting on a cornering vehicle. The first, and perhaps most simple, method is to simply use horizontal curvature data from the geometry table in the RAMM state highway database and a known velocity profile to calculate the centrifugal force. The relationship required for this is given in appendix A along with a more accurate form that accounts for gravity and curve super elevation.

Where road geometry data is not readily available (eg local authority roads), lateral accelerations during cornering can be directly measured with a vehicle instrumented with an accelerometer. The axis of the accelerometer is oriented horizontally and aligned perpendicular to the direction of travel to measure side thrust. By combining the measured lateral accelerations of the cornering vehicle with its mass, the lateral forces acting on the vehicle, and therefore the pavement, can be calculated.

A comparison of both methods for finding vehicle lateral accelerations, ie from raw geometry and by direct measurement, is shown graphically in appendix A for a representative section of SH58.

The final method investigated for determining lateral tyre forces occurring during cornering manoeuvres was using software that simulated a vehicle's interaction with the road geometry. Software was written with Matlab Simulink™, which through complex modelling of a vehicle's suspension and tyre/pavement interactions for specific geometries, permitted forces acting on each individual wheel of a cornering vehicle to be simulated. This software took as inputs the vehicle's path, physical dimensions, weight, centre of mass and suspension characteristics. From these inputs the program calculated the forces, both lateral and vertical, acting on each tyre. This method was selected for the first step in this research as it gave results for each tyre individually, thereby allowing a more in-depth investigation as to how wheel loads imposed by a vehicle during cornering related to chip loss.

The inputs used for these simulations were taken directly from on-road measurements involving an instrumented vehicle being driven around curves identified as having obvious and localised chip loss in one wheel path. The curve test sites were selected in the Hutt City suburb of Wainuiomata.

As paths taken through high-speed curves can vary dramatically from the centre-line geometry, an in-vehicle measurement system was used to measure the actual path taken by the test vehicle. The device used for measuring the path was an electronic compass, which measured bearings on three axes: heading, pitch and roll. The test vehicle was also fitted with a hubometer, which allowed distance travelled to be recorded from which speed through the curve could be derived. Both lanes of each curve test site were measured using the instrumented vehicle, which was a 1.5 litre, front wheel drive, Nissan Pulsar.

2.1 Simulation results

The data gathered from the test site measurements was input into the vehicle simulation software and the lateral and vertical tyre/pavement forces were calculated. The results of these simulations for the Nissan Pulsar are shown below in figure 2.1 for a representative site, site 7A, which was a right-hand curve traversed at a speed of 62km/h.

Details of this and the other test sites are provided in table B.1 of appendix B.

Figure 2.1 Vertical and lateral forces simulated for a Nissan Pulsar negotiating site 7A (refer table A.1). (LF – left front, RF – right front, LR – left rear, RR – right rear)

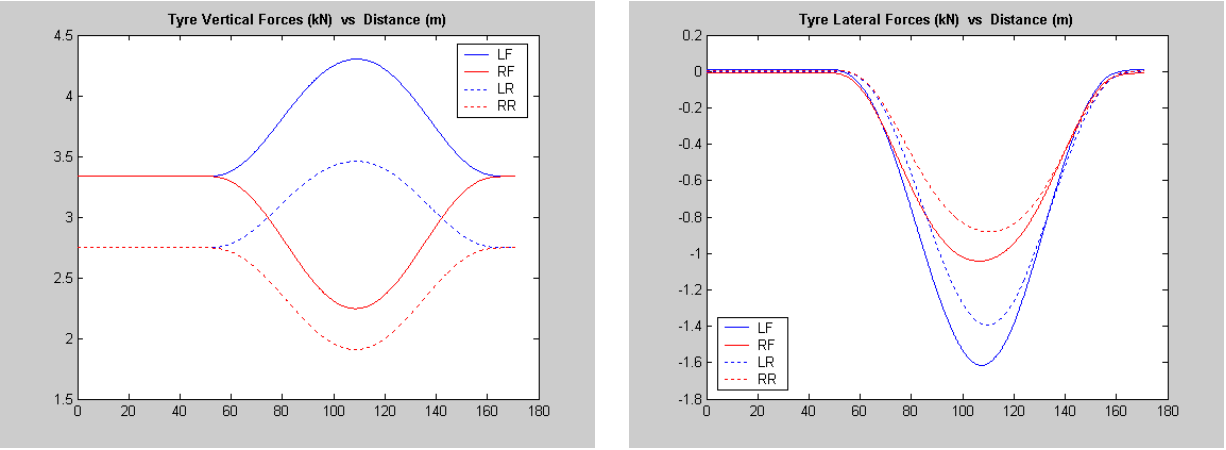

It was hypothesised the centre of the chip loss on a curve would be related to the location of the peak lateral force (PLF). With reference to figures B.4 to B.6 in appendix B, PLF always occurs on the outside wheel path of the curve, which is the left wheel path for a right-hand curve and the right wheel path for a left-hand curve. However, it was found, in the majority of cases, chip loss had occurred on the inside wheel path of the curve (ie right wheel path for a right-hand curve and left wheel path for a left-hand curve), which is opposite to the wheel path where maximum PLF occurs. This finding is attributed to the outside wheels being more highly loaded without slipping during cornering because of the vehicle body roll.

Accordingly, It was hypothesised that chip loss on a curve might be related to tyres with large lateral loadings combined with small vertical loadings. To test this hypothesis the maximum peak force ratio (PFR), defined as the lateral force divided by the vertical force, was correlated to the location of chip loss as shown in figure 2.2.

From figure 2.2 it can be seen there appears to be a strong correlation between the location of the PFR and the centre of chip loss. Furthermore, the PFR is located on the inside wheel path for cornering vehicles, which matches the location of chip loss occurrence at the majority of sites.

The methodology and analysis of this investigation into the relationship between tyre/pavement forces and chip loss is presented in greater detail in appendix B. Somewhat surprisingly there was a strong linkage, in the sites investigated, between the PFR and chip loss in one turn direction only, this being left.

Figure 2.2 Plot showing the correlation between the PFR and the location of chip loss

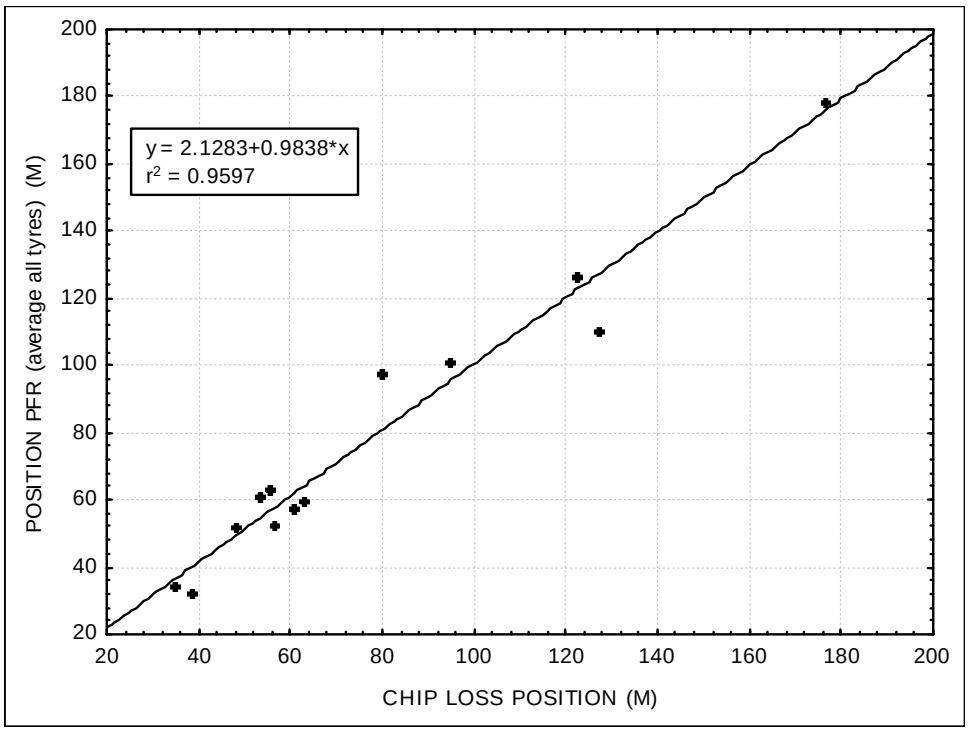

2.2 Discussion

The simulation results above suggest there is a link between high pavement stress and chip loss. To give further detail:

1 The maximum PLF is at the same *longitudinal* location but not in the same *transverse* location as the chip loss.

2 The maximum PFR occurs at the same location (both transverse and longitudinal) as the observed chip loss and so is a good indicator of where chip loss is likely, but

3 The linkage between a high PFR and chip loss appears true for one turn direction only.

Taken together, these findings infer that chip loss on chipseal surfacings occurs where high shear stress on the surface is generated from cornering vehicles. However, this should not be seen to imply the inverse, ie that where there is high shear stress, chip loss automatically occurs. In fact this is not the case, as can be seen from an inspection of the test sites and New Zealand road networks in general.

The question arising from this simulation-based study is whether the applied stress during cornering is sufficient to cause the bitumen binder to fail allowing chips to be stripped from the surface? If not, then there has to be at least one additional factor to shear stress that contributes to the relationship between shear stress and chip loss observed for the test sites.

3 Impact of traffic-induced shear stress

Following on from the previous section, a key question arises: is induced shear stress from cornering traffic sufficient to cause chip loss? In order to answer this question, three scenarios were investigated to determine the lateral and vertical tyre forces acting on a chipseal surface and then, using a finite element model, the shear stresses applied. The three scenarios investigated were:

1 A light vehicle (eg a car) and heavy vehicle (eg a truck) cornering at a speed sufficient to induce 85th percentile lateral accelerations

2 A light vehicle and heavy vehicle cornering at a speed sufficient to induce 99th percentile lateral accelerations

3 A truck cornering at slow speed so that scuffing forces were imposed on the road surface from the scrubbing action of the tyres.

3.1 Traffic-induced forces

3.1.1 Cornering velocity

It was hypothesised that the forces exerted by cornering vehicles remained reasonably constant irrespective of horizontal curvature. This could be explained by a vehicle's cornering speed decreasing as the curve radius decreased resulting in the lateral force acting on the vehicle remaining constant.

The curve advisory speed can be calculated from the curve radius and the crossfall using equation 3.1 (Koorey et al 2001). The curve speed and radius could then simply be related to the lateral accelerations induced on the vehicle using equation A.1 in appendix A. As the lateral acceleration is directly proportional to the shear force induced in the road surface, it was possible to gain an impression of how forces induced at the tyre-road interface during cornering varied with the horizontal radius of the curve.

$$AS = -\left(\frac{107.95}{H}\right) + \sqrt{\left(\frac{107.95}{H}\right)^2 + \left[\frac{127{,}000}{H}\right]\left[0.3 + \frac{X}{100}\right]} \qquad \text{(Equation 3.1)}$$

where AS = curve advisory speed (km/h)

H = absolute curvature (radians/km) = (1000/R), where R = curve radius (m)

X = absolute value of crossfall (%).

To ensure the speeds calculated were representative of realistic curves, crossfall values were taken from the *Austroads rural road design guide* (Austroads 1999). These crossfall values were limited to between 2% and 15% and were consistent with the guidelines given in section 4 of the draft *State highway geometric design manual* (NZTA 2005).

Therefore, the crossfall values were applicable to the New Zealand state highway (SH) network.

As the crossfall of the curve can have a large effect on the curve advisory speed, it was important to see how well actual crossfall values compared to theoretical values obtained from the *Austroads rural road design guide*. This was done by extracting the absolute crossfall of all rural curves on the SH network with radii tighter than 500m. Figure 3.1 shows the crossfalls, both theoretical (*Austroads rural road design guide*) and actual (New Zealand SH network) as a function of curve radius.

Figure 3.1 Actual versus theoretical crossfall values as function of curve radius

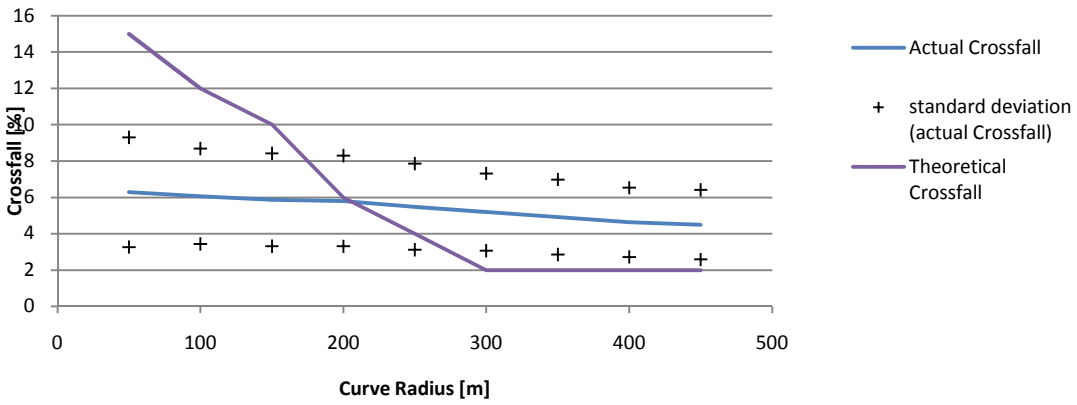

With reference to equation 3.2, the theoretical crossfall was calculated from the design curve speed and design friction value. No account was taken of the nominal speed environment. The consequence of this is that wherever the speed environment is less than the design curve speed, the theoretical crossfall will be greater than expected. Conversely, wherever the speed environment is greater than the design curve speed, the theoretical crossfall will be less than expected.

$$e = \left(V_d^2/127R_a\right) - f_d \qquad \text{(Equation 3.2)}$$

where e = theoretical crossfall (m/m)

V_d = design speed (km/h)

R_a = actual radius of curve (m).

f_d = design friction = 0.30 - 0.0017V_d

From figure 3.1 it can be seen the actual crossfall found on the SH network stays reasonably constant whereas the recommended design (theoretical) crossfall increases dramatically as the curve radius decreases from 300m radius onwards.

The values of actual and theoretical crossfall and curve radius shown in figure 3.1 were used as inputs to equation 3.1 to calculate the associated curve advisory speed. Figure 3.2 shows the resulting plots of curve speed versus curve radius.

Figure 3.2 Advisory curve speed against curve radius evaluated using theoretical and actual values for crossfall

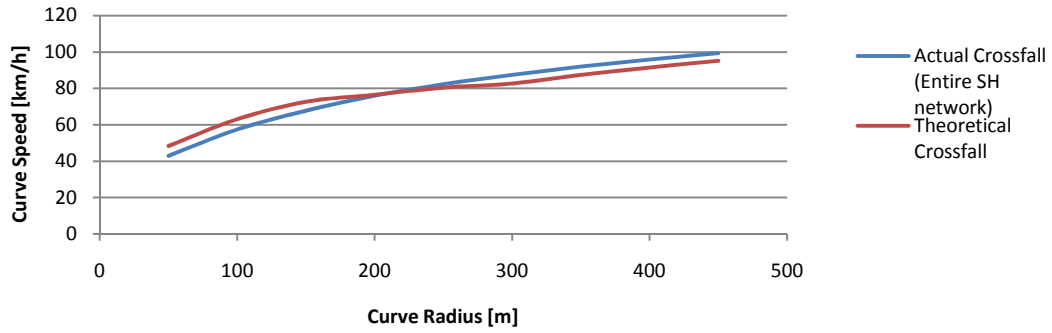

For the remainder of the investigation into the influence of road geometry on tyre/pavement forces, it was decided to use the curve speeds calculated from the actual crossfall values obtained from the New Zealand SH network rather than theoretical values. This was done for two reasons.

1 New Zealand road conditions are likely to be better reflected in any theoretical modelling.

2 The actual crossfall values are lower than the recommended design values. Therefore, the component of the lateral acceleration acting parallel to the road surface is larger and the component acting normal to the surface is smaller. It has been hypothesised, and shown in chapter 2 of this report, that chip loss can be located in areas where this type of loading combination is present. As a consequence, actual crossfall values are more likely to explain chip loss by this mechanism.

Equation 3.1 calculates the curve advisory speed. However not all vehicles will try to take a curve at this speed, which corresponds to the 85th percentile curve speed. Some drivers will try to negotiate the curve at significantly higher speeds, which will induce higher forces and so cause more damage to the road surface.

Expressions for converting the 85th percentile speed to the 99th percentile speed were derived from measured curve speed distributions of cars and trucks presented in Koorey et al 2001. The analysis performed has been summarised in appendix C and the resulting expressions for light vehicles and heavy vehicles are given as equations 3.3 and 3.4 respectively.

For light vehicles: $S_{99\%} = 37.19 + 0.8815 \times AS - 0.3652 \times AR$ (Equation 3.3)

For heavy vehicles: $S_{99\%} = 37.54 + 0.8328 \times AS - 0.3298 \times AR$ (Equation 3.4)

where $S_{99\%}$ = 99th percentile curve speed(km/h)

AS = curve advisory speed (km/h)

AR = average road roughness (NAASRA counts/km)

Equations 3.3 and 3.4 were evaluated using the curve advisory speeds calculated using the actual crossfall data obtained from the SH network. The average roughness was taken as 70 NAASRA representing a smooth road. This represents the worst case scenario as it leads to higher curve speeds and induced forces. The 99th percentile curve speeds for light and heavy vehicles are shown in figure 3.3.

Figure 3.3 99th percentile curve speeds plotted against curve radius for light and heavy vehicles

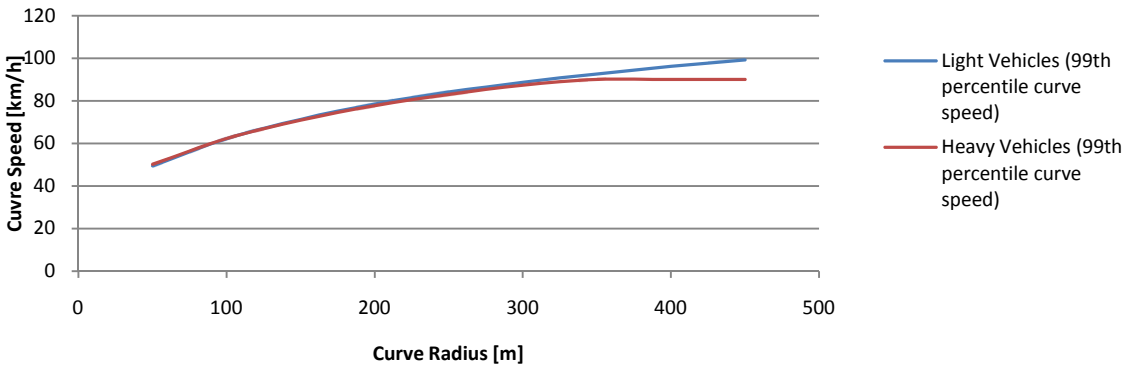

The levelling of the 99th percentile curve speed for heavy vehicles shown on curves of radius larger than 350m is due to the current speed restriction of trucks in New Zealand of 90km/h. Once the curve speeds are calculated the effect that both the geometry and curve speed have on the lateral forces exerted on the chipseal can be investigated. As the lateral acceleration is proportional to the lateral force, the lateral acceleration is a good way of investigating trends in lateral forces irrespective of vehicle mass. The lateral accelerations are simply calculated from the curve speeds using equation 3.5.

$$a = \frac{(CS/3.6)^2}{R} \qquad \text{(Equation 3.5)}$$

where a = lateral acceleration (m/s^2)

CS = curve speed (km/hr)

R = curve radius.

Equation 3.5 was evaluated using the advisory curve speeds calculated with the actual crossfall from the SH network, the 99th percentile curve speed for both light and heavy vehicles. The resulting lateral accelerations are shown in figure 3.4.

From figure 3.4 it can be seen the lateral accelerations, and therefore the lateral forces, are increased on curves of tighter radius.

This can be linked to the fact that crossfall increases as curve radius decreases and this increase in crossfall allows vehicles to travel faster. The lateral accelerations generated by vehicles travelling at the 99th percentile curve speed were found to be significantly larger than those generated at the curve advisory speed. Although the lateral accelerations generated by the light and heavy vehicles travelling at the 99th percentile curve speed are comparable, the forces generated by the heavy vehicles are higher due to their much larger mass.

Figure 3.4 Lateral accelerations generated by vehicles negotiating curves at different speeds

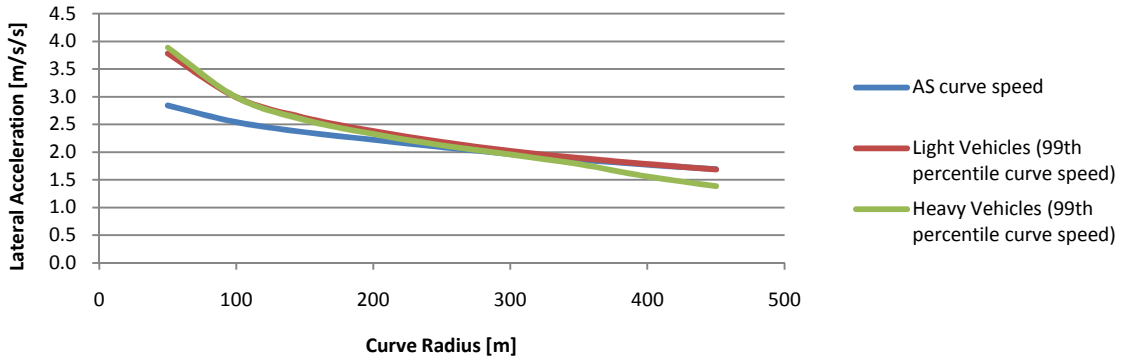

3.1.2 Tyre rolling and scrubbing forces on curves

When a truck or vehicle with a long wheel base attempts to negotiate a tight curve the un-steering wheels cannot make the turn required without the tyres exerting a scrubbing force across the road surface. Tyre scrubbing action is particularly noticeable on trucks with tandem axles and it is believed to be linked to chip loss on very tight curves, intersections and driveways. For consistency with the terminology used by Taramoeroa and de Pont (2008), the horizontal shear force that reacts to the applied tyre scrubbing force is referred to in this report as pavement scuffing force.

The previous section investigated the tyre/pavement forces induced by cornering vehicles assuming the tyres were still rolling rather than scrubbing. In the report by Taramoeroa and de Pont (2008), scuffing forces produced by heavy vehicles with multi-axle groups were investigated. The report found scuffing forces increased with decreasing curve radius and in field trials the scuffing forces generated were sufficient to cause abrasion to the road surface with small fragments being broken from the chipseal.

To obtain a picture of the forces acting on the chipseal on very tight curves, both the scuffing force (Taramoeroa and de Pont 2008) and the lateral force, calculated from the 99th percentile curve speed for heavy vehicles are shown in figure 3.5.

The scuffing forces presented in figure 3.5 were calculated assuming a tri-axle set with dual tyre carrying a vertical load of 29.42kN (3 tonnes). For the scuffing calculations the axle group spacing was taken as 3m and a wheelbase of 8.5m. For the lateral force calculation it was assumed the axle grouping would be responsible for reacting the 3 tonnes load, ie lateral force was calculated as F=ma where m = 3 tonnes and a is as in equation 3.4.

Figure 3.5 shows even the lateral forces generated by a heavy vehicle cornering at a 99th percentile curve speed is significantly smaller than the scuffing forces produced. Scuffing not only exerts significantly higher forces on the pavement but the sliding of the tyres can also ‘roll’ the chip out of the binder.

Figure 3.5 Lateral and scuffing forces for tight curves

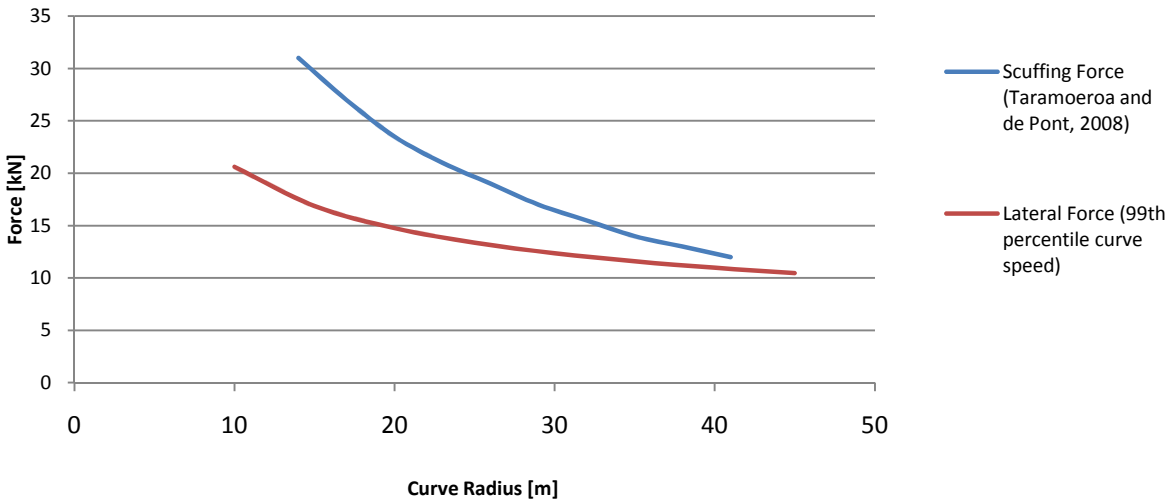

3.2 Finite element analysis of chip loss

3.2.1 Study design

The analyses performed in the previous section investigated pavement loads arising from the tyres of cornering vehicles. To build on the results of these investigations, the finite element investigation described below considered whether such pavement loads were sufficient to cause chip loss.

Specifically, a two-dimensional (2D) finite element (FE) simulation was performed to investigate whether the forces induced by cornering (ie including lateral forces but excluding scuffing forces) were sufficient to cause chip loss. FE simulations were performed on two different seal chip grades, grade 2 and grade 4, to establish the magnitude of the induced stresses and the differences in stress distributions between seal chip grades.

3.2.2 Methodology

3.2.2.1 Image preparation

The FE analysis was performed on two chipseal cores, one of grade 2 chipseal and the other of grade 4. The geometry used to create the computerised representation of the chipseal was taken directly from 2D images of the cores. For this, the sectioned cores were scanned at a resolution of 1200dpi, relating to a pixel size of 0.021mm, to generate bitmap images. Figure 3.6 shows an example of a chipseal core sample image.

A manual method was used to segment the chip (grey), the bitumen (black) and void (white). This segmentation was done using Paint Shop Pro® version 6.00 (Herrington and Henderson 2004). The specifications of the cores used are shown in table 3.1.

Table 3.1 Specifications of the two chipseal cores to be used for the FE analysis

Core identification	Location	Core diameter	Surface layer 1	Layer 2	Layer 3
Grade 2	SH2, RP 592/9.5	150mm	Grade 2 chip, laid 19/02/96	Grade 5 chip, laid 20/03/92	Grade 3 chip, laid 26/12/85
Grade 4	SH1S, RP 447/11.77	150mm	Grade 3 chip, laid 22/11/94	Grade 6 chip, laid 30/10/90	Grade 5 chip, laid 01/02/84

Figure 3.6 A typical chipseal core sample image after processing (vector format)

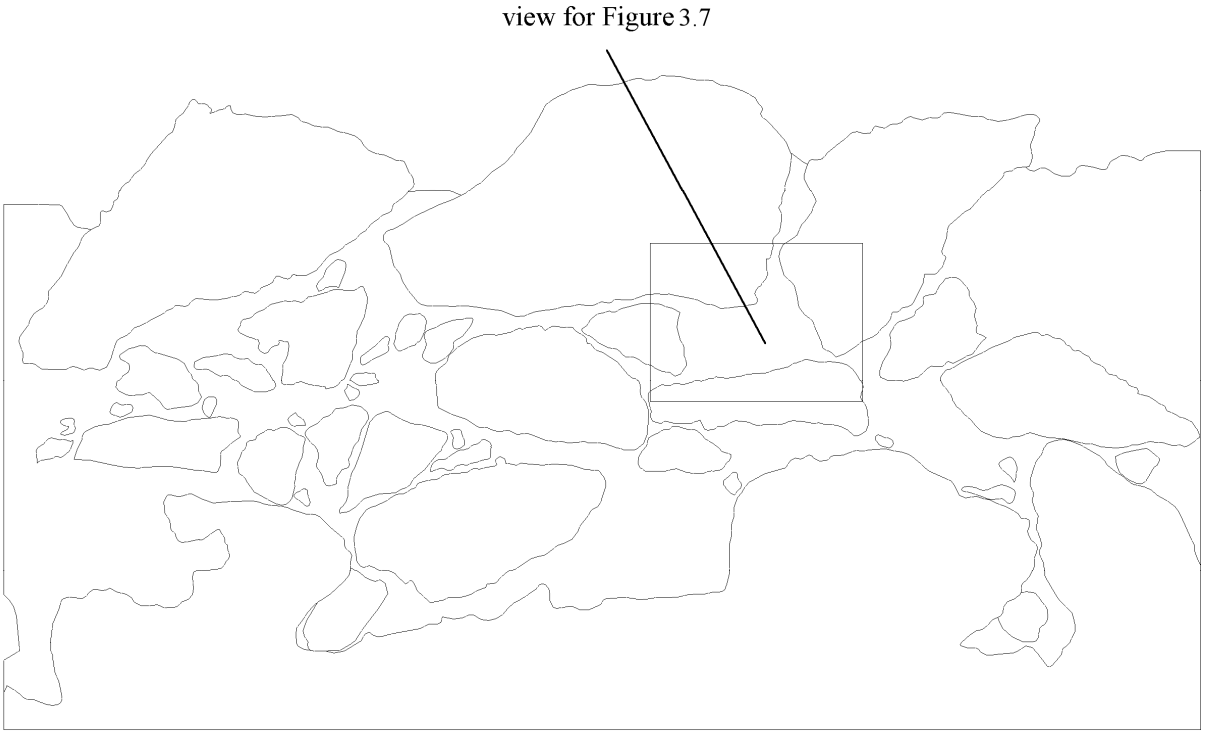

3.2.2.2 Loads imposed

The loads applied to models of both cores related to the maximum expected tyre loads for a truck negotiating a tight curve. These tyre loads were calculated with the following assumptions:

- The vehicle was a truck with tyres inflated to a pressure of 90psi (620.5kPa).
- The truck tyres were un-treaded.
- The truck was turning through a radius of 50m.
- Crossfall = 0%.
- Gradient = 0%.
- To obtain a lateral acceleration of 0.25g, a truck speed of 39.9km/h was assumed.
- The chipseal model was directly below the sidewall of the tyre (ie at the edge of the tyre) where the contact-patch forces are greatest.
- Forces exerted on the pavement through tyre scrubbing were not included in the simulation.

As it was found earlier that tyre/pavement loads were maximum for smaller radius curves, this modelling situation represented the highest pavement loads that could be expected. Also as the crossfall of the curve used in this simulation was zero, a greater proportion of the load would be lateral (acting in shear) which was thought to contribute more to chip loss than vertical loading.

Tyre to pavement loads can be separated into two components: those that are directly imposed by the truck and those that result inherently from the non-uniform distribution of stresses in the contact patch. The loads imposed directly by the truck were calculated for three orthogonal directions: vertical, lateral and longitudinal. These orthogonal components of the imposed load are outlined in table 3.2.

Table 3.2 Orthogonal components of load imposed by cornering truck

Load direction	Notes	Percentage of vertical load
Vertical	Equal to tyre inflation pressure.	100%
Lateral	Due to cornering.	Typically 25% (value used varied depending on lateral force)
Longitudinal	Due to aerodynamic drag and rolling resistance.	1%

It should be noted that the vertical load imposed by a tyre on the pavement is largely a function of tyre inflation pressure. Any increase in load applied from the truck results in a proportional increase in contact area rather than an increase in contact force. Thus, a lateral load transfer due to cornering results in an increase in contact patch size on the outside tyres and a smaller contact patch size on the inside tyres. However, the actual forces imposed on the pavement will remain similar in magnitude.

Once the loads imposed by the truck had been identified, the loads imposed by stress distributions in the contact patch could be investigated. Based on experimental data (de Beer 1994), the contact patch was assumed to be rectangular in shape with a length of 158mm and a width of 200mm. It was assumed the lateral load imposed on the tyre by the truck due to cornering did not affect the stress distribution shape due to the contact area itself. Consequently, the tyre to pavement lateral force due to cornering and the tyre to pavement lateral force due to the contact patch stress distribution were superimposed by adding. This may not have been true, but given the lack of experimental data, it was considered a reasonable assumption for this work.

The positions and magnitudes of the vertical tyre loads were calculated using the FORmula TRANslating (FORTRAN) code of Eberhardt and Clapp (Henderson et al 2005). This code predicts the actual contact area and contact pressure of a tyre on a pavement. The inputs required for the algorithm were the 2D texture profile of the pavement taken from the chipseal core scan, the inflation pressure of the tyre taken to be 90psi (620.5kPa) and the tread rubber stiffness of the tyre, taken as 5MPa.

3.2.3 Results

The FE analysis was performed on the chipseal scans with plain strain quadratic elements using the VISCO quasi-static analysis procedure provided by ABAQUS. The aggregate chips were modelled as rigid elements and the bitumen as a linear viscoelastic material represented by a Prony series. Further detail on the analysis procedure is given by Henderson et al (2005).

Table 3.3 summarises the results of the FE analysis for the truck negotiating a 50m radius curve at the 85th percentile speed of 39.9km/h, corresponding to a lateral acceleration of 0.25g. This data in turn has been used to derive maximum principal stresses for cornering accelerations corresponding to 0.4g and 0.5g tabulated in table 3.4.

Table 3.3 Maximum principal stresses calculated for grade 2 and grade 4 chipseal via FE analysis

Percent of the bitumen area exposed to a stress level greater than the tabulated principal stress level[a]	Maximum principal stress (MPa)	
	Situation: 85th percentile speed around curve of 50m radius ie 0.25g lateral acceleration	
	Grade 4	Grade 2
1%	0.215	1.592
5%	0.102	0.504
25%	0.032	0.117

[a] The FE model had a fine mesh of elements for the area of the bitumen in the chipseal. These values are the percentage of that total area that suffered a stress greater than the tabulated value of principal stress.

Table 3.4 Maximum principle stresses calculated for grade 2 and grade 4 chipseal via extrapolation of FE analysis simulations presented in table 3.3

Percent of the bitumen area exposed to a stress level greater than the tabulated principal stress level[1]	Maximum principle stress (MPa)			
	Situation: 99th percentile speed around curve of 50m radius ie 0.40g lateral acceleration		Situation: 15m radius taken at speed of 31km/h ie 0.50g lateral acceleration	
	Grade 4	Grade 2	Grade 4	Grade 2
1%	0.229	1.696	0.240	1.777
5%	0.109	0.537	0.114	0.562
25%	0.034	0.125	0.036	0.131

It will be noted that the maximum principal stresses tabulated in table 3.4 are not in the ratio of the vehicle lateral accelerations (ie 0.25:0.40:0.50) as the total applied tyre load consisted of three components (vertical, lateral and longitudinal) and the vertical and longitudinal components did not vary in proportion with the vehicle lateral acceleration. Therefore, the maximum principal stresses tabulated in table 3.4 have been estimated by the ratio of the 3D sum of the three load components at 0.25g with the 3D sum of the three load components at 0.4g and 0.5g.

Furthermore, the situation generating the 0.5g lateral acceleration may be unrealistic given the truck needs to travel at a relatively high speed of about 31km/h around a very tight (15m radius) curve. However, the 0.5g lateral acceleration may be achieved in practice by driving a non-constant radius path. The case of 0.5g lateral acceleration has been considered because it is taken to represent an upper extreme of expected lateral accelerations.

With reference to tables 3.3 and 3.4 and figure 3.7, it can be seen the peak stresses induced by the cornering truck are localised and tend to be concentrated in thin films of bitumen where aggregate chip surfaces are in close proximity. It was also found the stresses induced in the grade 2 chipseal were approximately five times higher than those in the grade 4 chipseal. This suggests that for high stress situations it may be worth considering the use of smaller sized sealing chips, ie grade 4 or higher.

Figures 3.7 Typical FE analysis stress distribution plots (area shown indicated in figure 3.6)

Figure 3.7a Von Mises stress at 0% of time for maximum tyre load

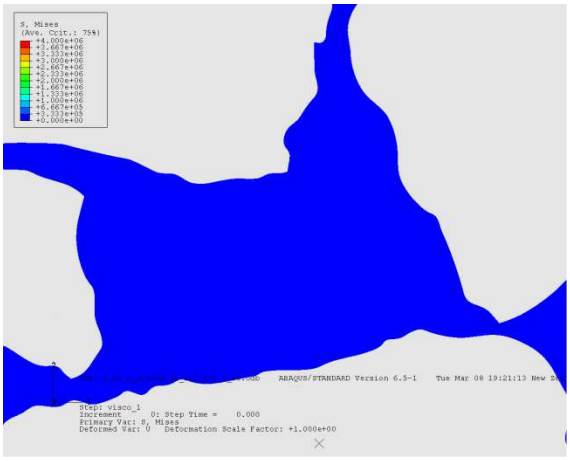

Figure 3.7b Von Mises stress at 18.5% of time for maximum tyre load)

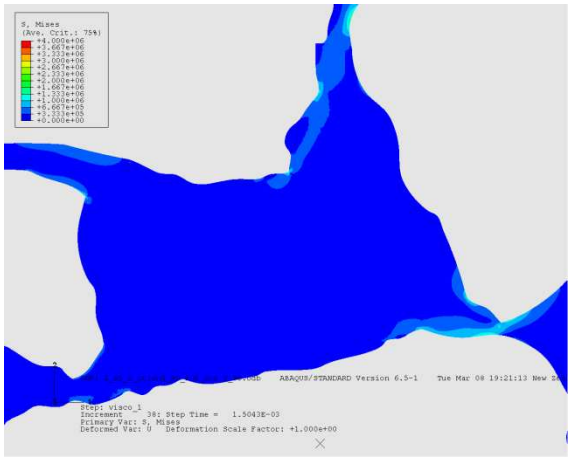

Figure 3.7c Von Mises stress at 49% of time for maximum tyre load

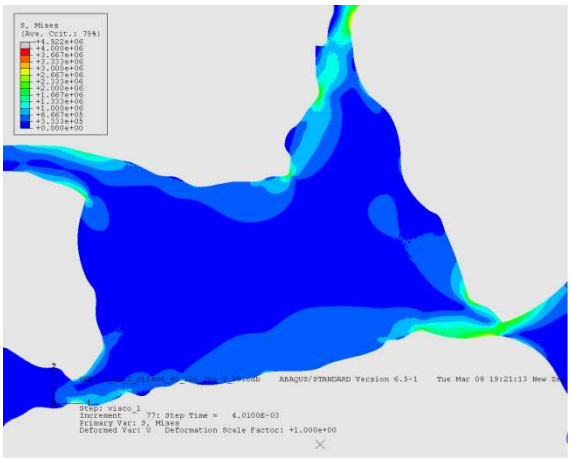

Figure 3.7d Von Mises stress at 100% of time for maximum tyre load

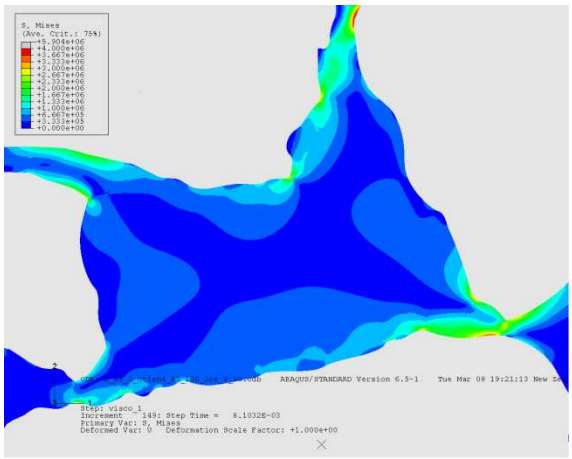

The inference that can be taken from tables 3.3 and 3.4 when comparing maximum principal stress levels experienced by 1% and 25% respectively of the bitumen area is that stresses in a loaded chipseal can be highly non-uniform, with the heavily stressed bitumen regions being extremely small. For the most part, typical bitumen stresses were significantly lower than the highest 1% of stresses.

The obvious question is, are the stresses tabulated in tables 3.3 and 3.4 sufficient to cause chip loss?

To investigate possible answers to this question the effects of confinement ratio, the viscoelastic/plastic nature of bitumen and bitumen stress test results had to be considered. The results are summarised in the following section.

3.3 Failure stresses in bitumen

According to published bitumen failure research (eg Herrington and Henderson 2004), the failure stress of bitumen is strongly influenced by specimen geometry, with failure occurring in specimens with a large diameter and a thin film at a higher stress level than specimens of identical diameter with a thick film. This geometry can be referred to as the 'confinement ratio', often defined as the ratio of diameter (d) of a cylindrical film to its length (l). Values for the confinement ratio reported by Herrington and Henderson (2004) in their study of chipseals typically ranged from 0.001 to 20. Perhaps primarily because of this effect of geometry, the stress fields noted in the FE analysis study described in the previous sub-section were observed to be highly non-uniform. The decision was therefore made to express stresses in terms of percentiles, rather than the maximum as the latter was thought to be highly dependent on the particular geometry of the chipseal cores chosen for study.

As mentioned briefly by Herrington and Henderson (2004), a further consideration was that the failure of a bitumen film under test is strongly load-rate dependent, with slower load application rates tending to result in the viscous/plastic nature of bitumen becoming apparent. Conversely, at higher load application rates, bitumen tends to behave more like a solid and its viscous nature is less apparent.

A final consideration was that bitumen behaviour is highly temperature dependent. For example, a chipseal that might fail by cracking at 5ºC under cornering tyre loads might simply deform (perhaps unacceptably) without cracking due to bitumen's non-solid behaviour at higher temperatures.

The question of how to define bitumen failure in chipseals arises from the preceding discussions. With the application of loads from cornering tyres, stresses in a small minority of thin films (where adjacent aggregate chips happen to be in close proximity) may be sufficient to cause localised bitumen over-stressing. However, the affected aggregate chips will potentially still remain supported in place by the less stressed bitumen. With the passage of time and temperature cycles of sufficient magnitude, the 'failed' areas of bitumen may heal.

3.4 Discussion

Taking the FE analysis results presented in sections 3.2 and 3.3 into account along with the results in Herrington and Henderson (2004), it is suggested, for the range of confinement ratios expected in chipseals, the failure of a well-constructed chipseal at temperatures of less than or equal to around 15ºC is unlikely. Even under the extreme condition of a truck tyre inflated to 90psi cornering at a sufficient speed to cause a lateral acceleration of up to or equal to 0.50g, failure in chipseals is unlikely to occur provided the temperature remains below 15ºC. However, there may be situations when the applied stress may be sufficient to cause bitumen overstressing in chipseals (eg at temperatures greater than around 15ºC). In these cases the bitumen might be over-stressed resulting in chip loss.

In situations where there is concern the applied stresses may be sufficient to cause chip loss, the use of a smaller sized chip (ie grade 4 or less) reduces the stress by almost an order of magnitude (refer tables 3.3 and 3.4).

As the FE analysis showed applied tyre loads as being unlikely to cause chip loss in chipseal surfaced curves, attention turned to investigating correlations between physical attributes of SH curves and chip loss in an attempt to identify possible causal factors.

4 Statistical regression model

4.1 Prediction models based on RAMM data

4.1.1 Study design

This statistical analysis was performed on data from the RAMM database which contains a wide variety of information on the New Zealand SH network. For the purposes of this investigation the data contained in the RAMM database was separated into five groupings:

- physical variables
- traffic variables
- temporal variables
- categorical variables associated with seal type and carriageway.

The original dataset was obtained from the New Zealand SH network and consisted of more than 630,000 entries describing 10m road sections with a horizontal radius of curvature less than 750m. To enable a more meaningful analysis to be performed, these 10m sections were aggregated by taking into account the interdependency of each 10m section with its immediate neighbours. In this way 65,000 curves were formed for analysis.

To understand the importance that each variable had individually to chip loss, a correlation was performed using the Pearson correlation for numeric variables and in the case of categorical variables using Phi or Cramer's V. A total of 33 variables comprising 28 numeric variables and five categorical variables from the RAMM database had their correlation to chip loss calculated. Once the variables with the highest correlation to chip loss had been identified, they were combined into a logistic regression model to give the best possible explanation of chip loss from the information available in the RAMM database. Analysis of the model then followed with checks on physical relevance.

4.1.2 Variable correlation

The first correlations performed were between the 25 numeric variables and the chip loss variable. These were done using Pearson correlation. Following this, the five categorical variables were correlated with the chip loss variables using Cramer's V. The results for both sets of correlations are shown below in tables 4.1 to 4.4. For the numeric variables, the mean, standard deviation (SD) and sample size (N) are tabulated in addition to the Pearson correlation.

Variables with abbreviated names are defined in the glossary, see appendix D.

Table 4.1 Pearson correlation between several physical variables and chip loss

	Physical variables	Mean	SD	N	Correlation with chip loss
1	chip_size	3.34	1.34	65,901	-0.057
2	average_dim	8.74	2.3	13,593	0.056
3	chip_2nd_size	4.66	0.62	20,252	-0.049
4	polished_stone_value	56.04	4.13	16,790	0.115
5	lane_texture_depth	1.90	0.61	65,901	0.013
6	skid_reporting_value (rv)	0.11	0.1	68,476	-0.039

	Physical variables	Mean	SD	N	Correlation with chip loss
7	skid_site_category	3.71	0.72	68,476	0.02
8	surfacing_depth	0.14	2.82	65,901	-0.007
9	surfacing_width	8.59	2.21	57,057	0.019
10	carriageway_width	8.5	2.4	68,338	0.041
11	curvature	-1.8	462.19	68,593	0.005
12	crossfall	-0.36	4.99	68,593	-0.014
13	gradient	-0.31	4.17	68,593	-0.004

Table 4.1 shows very low correlation between curvature and chip loss. This result reinforces the findings observed previously in the report that while chip loss occurs at locations of high stress on curves, curves themselves are not a good predictor of chip loss.

Table 4.2 Pearson correlation between traffic-related variables and chip loss

	Traffic variables	Mean	SD	N	Correlation with chip loss
14	traffic_adt_count	6298.24	11911.54	19486	0.184
15	traffic_adt_estimated	3985.37	7647.59	67892	0.094
16	loading_percent_heavy	11.56	8.72	68338	0.004
17	loading_esa_heavy	1.1	0.25	68338	0.079
18	combined_traffic_adt	4043.52	7828.59	67932	0.09
19	LCV	1686.74	2813.29	67932	0.068
20	CLCV	2924355	7010134	65517	0.025
21	HCV	156.08	218.31	67932	0.089
22	CHCV	276419.8	573958.6	65517	0.032
23	HCVL	182.32	273	67932	0.093
24	CHCVL	321694	705557.9	65517	0.037
25	85%ile curve speed (CS)	92.66	18.26	68593	0.016
26	Lateral acceleration (LA)	-0.03	1.87	68593	0

The parameter *combined_traffic_adt* is the sum of light commercial vehicle (LCV) passes per day and the product of heavy commercial vehicle (HCV) passes and the number of equivalent standard axle (ESA) loads of 8.2 tonnes to provide an estimate of the total load on the pavement. The 85th percentile curve speed (CS) and estimated cornering lateral acceleration (LA) were calculated using equations 3.1 and 3.4 respectively. As can be seen from table 4.2, the standard traffic measure of average daily traffic (ADT) correlates the strongest with the occurrence of chip loss, whether estimated or counted.

Table 4.3 Pearson correlation between temporal variables and chip loss

	Temporal variables	Mean	SD	N	Correlation with chip loss
27	Month of sealing	5.96	4.7	3095	0.077
28	Seal age (days)	1837.6	1439.89	65901	-0.027

Table 4.4 Cramer's V correlation between categorical variables and chip loss

	Variable	Relationship with stripping
29	Carriageway area	0.499
30	Pavement source	0.371
31	Seal type (ie reseal, coat1 etc)	0.103
32	Carriageway hierarchy	0.088
33	Lane (ie L1, R1 etc)	0.08

Of the 33 variables from the RAMM database very few failed to correlate using basic analyses. However, the correlation of all but a few of the variables was found to be very weak, the strongest being the network region in which the curve was located (ie carriageway area in table 4.4).

4.1.3 Alternative models

In a physical sense, chip loss is undoubtedly related to the passing of vehicles (ie trafficking), so the finding that the variance in chip loss can be mostly explained by three categorical variables that are only roughly correlated to vehicle passes is troublesome. To try to obtain models that placed more emphasis on the passing of vehicles, additional models were created. These models employed traffic variables, curve variables and a combination of traffic and curve variables. Tables 4.6 and 4.7 show the coefficients and variables used to generate the models containing traffic only and curve only variables.

In these tables the weighting each variable has been given in the model (B), along with the significance of each variable to the model given by the standard error (SE), the Wald values (used to determine whether an effect exists or not), the level of significance and the exponential of B.

The variables have been banded.

These models were found to account for a relatively small amount of variation in chip loss. The model containing traffic variables explained 11% of the variance in chip loss (NegelKerke-R^2= 0.11), whereas the model containing curve geometry features explained 3.8% of the variance in chip loss (NegelKerke-R^2 = 0.038). The model combining traffic and curve geometry variables showed no significant overall improvement, as was expected from the poor performance of the curve geometry model.

The main result of this statistical analysis was that chip loss could not be explained by RAMM database variables that related to physical features. However, it was found the region where the curve was located was essential in any explanation of chip loss.

Table 4.6 Model using only variables relating to traffic

Variable	B	SE	Wald	Significance	Exp(B)
Constant	-2.371	0.126	356.269	0.000	0.093
traffic_adt_est_BND	0.347	0.025	199.289	0.000	1.415
comb_traffic_adt_BND	-0.377	0.046	66.496	0.000	0.686
CLCV_BND	-0.192	0.031	37.687	0.000	0.825
traffic_adt_count_BND	0.276	0.049	31.758	0.000	1.317
HCV_BND	-0.196	0.043	20.969	0.000	0.822
CHCVL_BND	0.211	0.050	17.778	0.000	1.235
loading_pc_heavy_BND	0.053	0.015	12.922	0.000	1.055
loading_esa_heavy_BND	0.032	0.012	6.647	0.010	1.032

Variable	B	SE	Wald	Significance	Exp(B)
AS_BND	-0.016	0.007	4.548	0.033	0.984
ECF_BND	-0.009	0.007	1.415	0.234	0.991
HCVL_BND	0.040	0.048	0.691	0.406	1.040
CHCV_BND	-0.014	0.048	0.087	0.768	0.986

Table 4.7 Model using only curve variables

Variable	B	S.E.	Wald	Significance	Exp(B)
Constant	17.053	8196.282	0.000	0.998	25471272.772
polished_stone_BND	0.203	0.011	315.446	0.000	1.225
surf_width_BND	0.184	0.018	100.543	0.000	1.202
cway_width_BND	-0.150	0.018	70.775	0.000	0.861
average_dim_BND	0.073	0.020	14.169	0.000	1.076
crossfall_BND	-0.030	0.014	4.859	0.027	0.970
curvature_BND	0.032	0.015	4.293	0.038	1.032
gradient_BND	0.010	0.010	1.034	0.309	1.010
chip_2nd_size_BND	0.079	0.085	0.855	0.355	1.082
chip_size_BND	0.025	0.068	0.136	0.712	1.026
surf_depth_BND	-20.096	8196.282	0.000	0.998	0.000

4.1.4 Interim discussion

These statistical models appeared to indicate there were no clear links between chip loss and the data held in the RAMM database, aside from possibly the NZTA administration region in which the curve was located.

Accordingly, the relationship between chip loss and the NZTA administration region warranted further consideration. This was achieved by way of developing a logistic regression model as described below.

4.2 Logistic regression model

To form the best possible explanation of chip loss from the data available from the RAMM database, a stepwise forward conditional logistic regression was performed on the 10 variables showing the highest correlation. Variables were entered and the estimates were achieved within 10 iterations of the maximum likelihood algorithm. The final model was created using seven interval variables and three categorical variables.

The results of this model are given in table 4.8. It shows the model correctly predicted just over a third of the curves that were observed to have chip loss (ie 4491 predicted against 12,238 observed).

Table 4.8 Classification table comparing the observed and predicted values of chip loss

		Total observed	Observation as percentage of total	Predicted stripping		Percentage correct
				NO	YES	
Total predicted		65,514		58,737	6777	
Observed stripping	**NO**	53,276	81.3%	50,990	2286	95.7%
	YES	12,238	18.7%	7747	4491	36.7%

The overall correct prediction was 84.7%. This percentage was made up of 50,990 curves where no stripping was correctly predicted plus a further 4491curves where stripping was correctly predicted equating to 55,481 curves out of a total of 65,514. Such a level of accuracy, when examined against the proportional chance criterion and the maximum chance criterion, was significantly above chance (see table 4.9).

The 'proportional chance' criteria for assessing model fit was calculated by summing the squared proportion for each sample group (ie the proportion of the sample in the 'observed chip loss' group and the 'no observed chip loss' group). The 'maximum chance' criterion was based on the proportion of cases in the largest group (in this case the no observed chip loss group). The maximum chance criterion was primarily used to take into account the uneven group size, which was a problem of this sample.

The classification accuracy achieved must exceed the proportional and maximum chance values by 25% to ensure the model has practical significance (see Hair et al 2010). However, the 84.7% accuracy level achieved did not exceed the final thresholds of predictive accuracy required (refer table 4.9). Therefore, the model could not be considered sufficiently robust for pavement management purposes.

Table 4.9 The proportional chance and maximum chance criterion values to test the assumption that the model predicts at a level above chance

Criterion	Calculation	%	Practical significance multiplier	Final threshold of predictive accuracy required
Proportional chance	$(0.813^2 + 0.187^2)$	69.6%	1.25	87.0%
Maximum chance	0.813	81.3%	1.25	101.6%

One concerning aspect of this analysis is the large amount of variance explained by the variable 'carriageway_area' which is a 'dummy' or categorical variable and represents the NZTA administration region in which the curve is located.

To further investigate the correlation between carriageway_area and chip loss, the model was fitted to each of the NZTA administration regions separately. Table 4.10 shows the resulting fits in terms of coefficient of determination (R^2) values for each independent region. As can be seen in table 4.10, the model gave mixed results, accounting for 91% of the variance in PSMC001 while only achieving 28% in Southland.

Table 4.10 Application of chip loss model to each NZTA administration region

North Island regions	R^2	South Island regions	R^2
Northland	0.90	Nelson	0.72
PSMC 005	0.63	Marlborough	0.58
Auckland	0.31	North Canterbury	0.41
West Waikato	N/A	South Canterbury	0.43
PSMC 001	0.91	Buller	N/A
East Waikato	0.85	Greymouth/West Coast	0.63
Central Waikato	0.35	Central Otago	0.38
Tauranga	0.75	Coastal Otago	0.43
Bay Road	0.89	Southland	0.28
BOP	0.42		
Rotorua	0.79		
Gisborne	0.34		
Napier	0.54		
West Whanganui	0.42		
East Whanganui	N/A		
Wellington	N/A		

4.2.1 Discussion

The results of the logistic regression modelling suggest for some NZTA administration regions, variables contained in the RAMM database can be a good predictor of chip loss. Specifically, while the logistic regression model was not particularly good at identifying where chip loss should occur when all regions in New Zealand were considered (36.7% accuracy, table 4.8), when applied at regional level it yielded R^2 coefficients of up to 0.91 (refer table 4.10). These results suggest in some regions, such as PSMC001, the traffic and physical variables in RAMM gave a good correlation to the chip loss sites. Conversely in other regions, such as Southland, the traffic and physical variables did not give a good correlation. In these areas some other factor was affecting the presence of chip loss.

In conclusion, the statistical modelling confirmed there are *regional* differences in the drivers of chip loss. There is a range of potential reasons for this which include climate, sealing chip properties and construction practices.

5 Influence of construction practices on chip loss

As concluded in chapter 4, regional variances when investigating chip loss could include construction practices. Accordingly, Towler and McCoy (2009) *Traffic management for resurfacing in the Wanganui region* investigated this potential factor. The abstract states:

> *The Wanganui Region of the NZ Transport Agency (previously Transit New Zealand) requires positive traffic management controls for a minimum period of 48 hours following chipseal resurfacing. This requirement, in use in Wanganui Region chipseal resurfacing contracts since the year 2000, has reduced the chipseal defects of scabbing and stripping by approximately 65%.*

This abstract appears to arise partly from the observations that:

> *... some chip loss occurs soon after construction and is related to construction deficiencies, e.g. dirty chip, lack of adhesion agent, excess traffic speeds during or soon after construction. Further chip loss can occur during normal service or if rain falls immediately after sealing.*

Other contributors to scabbing and stripping are thought to include over-chipping and stress caused by turning traffic (especially when there are high volumes of heavy traffic).

5.1.1 Discussion

To return the focus to this report and the question of whether construction practices can be a factor in chip loss, the indication from Towler and McCoy (2009 is that there is a linkage between construction practices and chip loss. Specifically, ensuring temporary traffic management is in place in the first 48 hours after pavement construction to limit traffic speeds to between 20km/h and 50km/h and also progressively move the traffic across the full width of the new seal, appears to significantly reduce the occurrence of chip loss. This is thought to be related to the packing and embedment of the aggregate chips.

6 Discussion of results

6.1 Overview

While chip loss is found where pavement stress induced by cornering vehicle tyres is high, high stress alone is not a good predictor of chip loss as shown in sections 2 and 4 of this report.

It is therefore hypothesised that chip loss in chipseal surfacings is a function of at least two factors:

- stress-induced failure of bitumen binder
- packing and embedment of aggregate chips.

Given the low correlation between high stress and chip loss (refer table 4.2) and the implied relatively high correlation between packing/embedment and chip loss reported by Towler and McCoy (2009), it is felt the latter (ie chip embedment and packing) is the dominant factor of the two in influencing chip loss. This emphasises the need to achieve compaction of the total width of the chipseal surface during the first 48 hours of a new seal through controlled trafficking.

To further reduce the likelihood of chip loss on high-stress curves, the use of smaller (ie grade 4 or 5) chips should be considered. However, this observation is made on the basis of FE analysis of only two, single coat chipseal surface cores, and analysis of many more cores would be required for a wide range of curve geometries, speeds and vehicles to establish this conclusively. It is also noted that when considering adopting this possible counter-measure, the increased potential for flushing from choosing to use a small aggregate chip would need to be weighed up in any decision.

On curves, superelevation (ie camber) helps to counterbalance the lateral acceleration of vehicles thereby reducing the horizontal stresses applied to the chipseal surface (refer appendix A). With reference to figure 3.1, there also appears to be scope for reducing the occurrence of chip loss on tight (ie horizontal radius less than 300m) curves through ensuring the superelevation is at the recommended design level for the curve radius.

In highway design, the amount of superelevation (ie crossfall angle) is chosen so the load of the inside wheels can be maintained at half the weight of the vehicle in the presence of lateral acceleration (Gillespie 1992). Given the radius of turn and an intended travel (design) speed, the design superelevation will generally produce a lateral acceleration in the range of zero to 0.1g.

6.2 Summary of key discussion points

The key discussion points arising from the research are summarised below by report chapter.

- Chapter 2 investigated tyre forces generated through cornering by on-road measurements and computer simulations. The discussion centred on chip loss on curves not generally occurring in the outer wheel path where the magnitude of the peak lateral force is greatest but rather the inner wheel path where the ratio of lateral to vertical force is greatest. The point was also made that while chip loss on chipseal surfacings coincides with where high pavement stress is generated from cornering vehicles the converse does not apply. Therefore, one cannot assume chip loss will automatically occur where cornering stresses are large.
- Chapter 3 investigated both 1) the issues around forces induced by cornering vehicles and 2) the consequences of these forces on FE simulated stresses in chipseal pavements. The FE simulation results suggest applied stresses from a cornering truck are unlikely to cause bitumen overstressing in

chipseals, even at lateral acceleration levels five times normally expected (ie 5g cf 0.1g). Furthermore, a possible mitigation measure, if this is found to be a problem, is to use small sized roading chip. However, it is observed that chipseal aggregate grade cannot be the sole factor in chip loss otherwise we would see a significantly higher proportion of chip loss failures on chipseal surfaces constructed of larger-sized aggregates (ie grades 2 and 3) compared with chipseal surfaces constructed from smaller-sized aggregates (ie grades 4 to 6).

- Chapter 4 investigated chip loss relationships by means of statistical models using the traffic or physical attributes of the surfacing held in the RAMM database. No strong relationships between any RAMM variables were identified aside from the RAMM database variable 'region,' which corresponds to the NZTA administration regions. Some regions had a high correlation between certain variables in the RAMM database and chip loss while others did not. This led to a hypothesis that there could be some regional factors that affect chip loss. These could include climate, sealing chip properties and construction practices.
- Chapter 5 investigated the findings of Towler and McCoy (2009) relevant to chip loss mitigation. The reference indicates that the occurrence of chip loss on chipseal surfaces can be significantly reduced through controlled trafficking in the first 48 hours after pavement construction by using temporary traffic management to reduce speeds to below 50km/h and to progressively move the traffic forwards and backwards across the full width of the new seal. It is thought this reduction in chip loss brought about by using controlled traffic for compaction is related to the improved packing and embedment of the sealing chips.

7 Conclusions and recommendations

The following conclusions and associated recommendation are the outcome of this research project which was undertaken to better understand chip loss on curves surfaced with chipseal..

7.1 Conclusions

1 If chip loss is observed on curves, it tends to occur where large lateral tyre loading is combined with small vertical tyre loading. This corresponds to the tightest part of the curve in the innermost wheel path.

2 It was determined from finite element modelling that even at lateral accelerations five times the level normally expected for properly designed curves, the stresses generated in single coat chipseals were insufficient to cause failure of the binder in large enough areas to cause chip loss.

3 The statistical modelling identified that chip loss on curves correlated strongest with the NZTA administration region. Further investigation using logistic regression modelling suggested that in some regions, traffic, curve geometry and seal-related variables stored in the RAMM database were a good predictor of chip loss, whereas in other regions this was not the case. This suggests there are regional differences in the drivers of chip loss. There is a range of potential reasons for this result which include climate, sealing chip properties and construction practices.

4 Taken overall, the research found there were two principal factors influencing chip loss induced by cornering vehicles:

   a bitumen failing from the induced stress

   b packing and embedment of the pavement surface layer aggregate chips.

   Of these two factors, the dominant one is aggregate packing and embedment. Therefore, the research supports previous findings that it is not the seal design but construction practices, notably the use of controlled traffic to bed the sealing chips, which have the greatest influence in mitigating chip loss.

7.2 Recommendations

1 Attention should be paid to ensuring surface compaction by controlling trafficking in the 48-hour period after chipseal construction to reduce the likelihood of chip loss.

2 Where there is a concern over chip loss, consideration should be given to the use of smaller chip sizes to reduce the stress in the bitumen, but this has to be weighed up against the potential for flushing.

3 On curves, superelevation (ie camber) helps to counterbalance the lateral acceleration of vehicles, thereby reducing the horizontal stresses applied to the chipseal surface. Therefore, there is additional scope for reducing the occurrence of chip loss on tight (ie horizontal radius less than 300m) curves through ensuring the superelevation is at the recommended design level for the curve radius.

4 The finite element simulations performed suggested the forces induced by cornering traffic may be insufficient to cause failure in the bitumen binder of well constructed roads in some situations. To confirm this, additional finite element simulations should be performed for a wide range of vehicle types, curve radii and superelevatiions, vehicle speeds, tyre inflation pressures and pavement aggregate grades. Such a study would also help to either support or negate the finding that the induced stress in chipseal surfacings decreases with increasing aggregate grade.

5 A limited analysis of vehicle speeds around curves with a horizontal radius of curvature ranging from about 30m to 215m resulted in two unexpected findings. The first was that lane roughness had a significant influence on the curve speed. The second was that the 99th percentile curve speed of heavy commercial vehicles was the same as that of passenger cars. Given the significance of these findings for speed management and surfacing design, a more comprehensive investigation of vehicle speed distributions on tight curves should be undertaken to establish robust relationships for estimating different percentile curve speeds as a function of vehicle class.

8 References

Austroads (1999) *Rural road design: a guide to the geometric design of rural roads*. AP-1/89. Sydney: Austroads.

Austroads (2000) *Guide to the selection of road surfacing*. AP-63/2000. Sydney: Austroads.

Ball, GFA (1998) Surfacing for high stress areas. *Transfund NZ research report 126*.

Cenek, PD, RB Davies, MW McLarin, G Griffith-Jones and NJ Locke (1997) Road environment and traffic crashes. *Transfund NZ research report 79*.

de Beer, M(1994) Measurement of tyre/pavement interface stresses under moving wheel loads. *Vehicle-Road and Vehicle-Bridge Interaction Conference*, Noordwijkerhout, The Netherlands.

Gillespie, TD (1992) *Fundamentals of vehicle dynamics*. SAE.

Hair, JF, WC Black, BJ Babin and RE Anderson (2010) *Multivarite data analysis*. 7th ed. London: Pearson Prentice Hall.

Henderson, RJ, P Herrington and J Patrick (2005) Finite-element modelling of a chip seal surfacing. Submitted for review and possible publication in: ARRB Transport Research, Road and Transport Research Journal.

Herrington, PR and RJ Henderson (2004) Bitumen film thickness and confinement ratios in chip seal surfacings. Road materials and pavement design: scientific note. *International Journal of Road Materials and Pavement Design 5*, no.2.

Koorey, GF, SJ Page, PF Stewart, J Gu, AS Ellis, RJ Henderson and PD Cenek (2001) Curve advisory speeds in New Zealand. *Transfund NZ research report 226*.

New Zealand Transport Agency (NZTA) (2005) State highway geometric design manual (draft). Accessed November 2011 from *www.nzta.govt.nz/resources/state-highway-geometric-design-manual/shgdm.html*

Taramoeroa, N and J de Pont (2008) Characterising pavement surface damage caused by tyre scuffing forces. *Land Transport NZ research report 374*. 66pp.

Towler, J and R McCoy (2009) Traffic management for resurfacing in the Wanganui region. *NZ Transport Agency & NZIHT 10th Annual Conference*, Rotorua, November 2009.

Appendix A: Calculation of lateral accelerations

Lateral accelerations induced by a cornering vehicle can be calculated directly from curve radius and crossfall data held in the road geometry table in the NZTA's RAMM database.

Assuming the velocity of the vehicle is known, the lateral acceleration can be calculated using the following formula:

$$a=V^2/(12.96\times R) \qquad \text{(Equation A.1)}$$

where a = lateral acceleration due to cornering (m/s^2)

V = linear velocity of cornering vehicle (km/h)

R = horizontal radius of curvature (m)

Equation A-1 can be modified to take into account the effect of superelevation on the lateral accelerations exerted on a cornering vehicle as shown in equation A.2.

$$a=(V^2/(12.96\times R)) - (g\times(SP/100)) \qquad \text{(Equation A.2)}$$

where g = gravity (9.81 m/s^2)

SP = superelevation (%)

Figure A.1 provides a graphic comparison of lateral accelerations calculated using equation A.2 and those measured with a vehicle-mounted accelerometer for a 3km section of SH58, which is located in the Wellington region.

From figure A.1 it can be seen the geometry calculated lateral accelerations agree very closely with the measured accelerations. Therefore, it is reasonable to conclude the road geometry data held in the RAMM database could be used to assist in the location of high-stress corners on the state highway network. This would do away with the need to directly measure lateral accelerations using a vehicle instrumented with accelerometers.

Figure A.1 Measured and calculated lateral accelerations for SH58

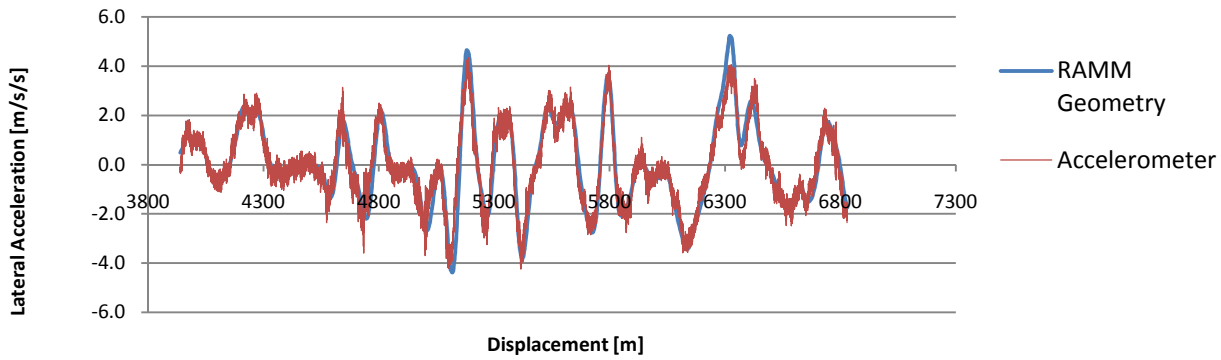

Appendix B: Test site tyre force distributions

B.1 Site selection

The sites used for the initial research for this project were located in suburban Wainuiomata and surrounding rural roads. These sites are listed in table B.1. The rural roads, Wainuiomata Coast Road and Moores Valley Road, had speed limits of 100km/h. Traffic volumes on these roads ranged from tens to thousands of vehicles per lane per day and most of the surfaces were grade 2 or grade 4 chipseal. Suitable sites could not be found on state highways in the Wellington region due to chip loss already being patched or because of their location on complex geometries such as the Rimatuka Hill Road. In most cases the lane not containing chip loss was also run for comparison and labelled with 'A' in table B.1.

Table B.1 Sites used for measuring geometries and traffic speeds

Site	Location	Turn direction	Speed (km/h)
4	200 Wainuiomata Coast Road ('big dip')	Left	76
4A		Right	78
7	North of park entry, Wainuiomata Coast Road	Left	65
7A		Right	62
81	217 Wainuiomata Coast Road	Left	63
81A		Right	62
82	217 Wainuiomata Coast Road	Left	63
82A		Right	62
9	475 Wainuiomata Coast Road	Left	80
9A		Right	79
10	437 Wainuiomata Coast Road	Left	81
10A		Right	79
15	Wainuiomata, Peel Place to Wood Street.	Left	25
16	Wainuiomata, Wood Street to Faulke Avenue	Left	30
17	264 Moores Valley Road	Left	68
17A		Right	67
18	370 Moores Valley Road	Right	67
18A		Left	65
21	423 Moores Valley Road	Right	69
21A		Left	70
22	471 Moores Valley Road	Left	65
22A		Right	61
23	Wainuiomata, Moohan Street to Wright Street	Left	28

B.1.1 Measurement of site geometry

The Matlab Simulink™ software used to calculate the tyre to pavement cornering forces requires as inputs both the path followed by the vehicle through the curve and the speed of the vehicle through the curve. In the case of high-speed curves the actual path taken by traffic can differ dramatically from the 'theoretical' path. Due to this, and because data from recent SCRIM surveys was not available for all the sites, the path

of an actual vehicle traversing the site was measured using an electronic compass. The compass was a Honeywell HMR3000 which measured angles on three orthogonal axes relating to heading, pitch and roll. The compass had problems with drift caused by the body of the vehicle but this was measured and calibrated for. The speed of the vehicle was measured using a hubometer. The final data used for the software was the average of two or three runs. Figure B.1 shows an example of the calibrated heading data from the compass.

Figure B.1 Calibrated heading data for site 7 obtained using an electronic compass

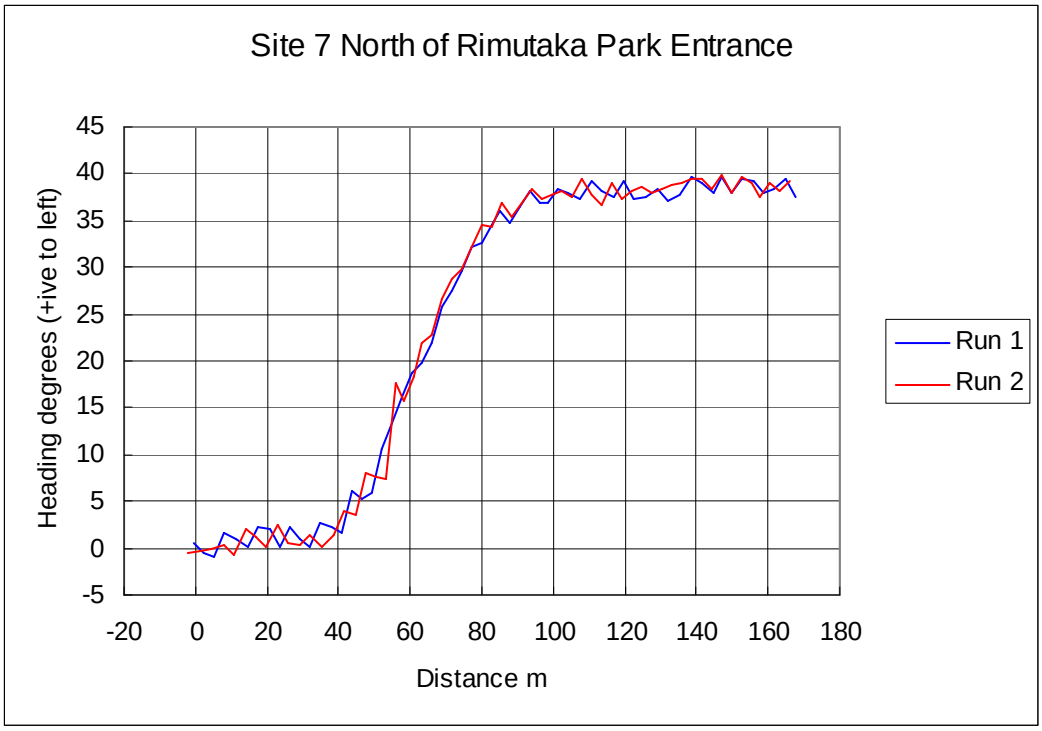

B.1.2 Vehicle simulation software

The vehicle simulation software was written in Matlab Simulink™. The vehicle path was measured using the electronic compass as described above and it was found that in all cases the measured trajectory could be approximated using a single cycle haversine steer angle of appropriate amplitude and frequency. The speed input into the software was constant and equal to the speed at the point of chip loss on each curve. The software also required vehicle parameters such as physical dimensions, weight, centre of gravity and suspension characteristics. Once all the inputs were entered, the software 'drove' a virtual vehicle around each of the curves and calculated the horizontal and vertical forces acting on each tyre. All sites were simulated using a 1.3 litre, front wheel drive Nissan Pulsar and some sites had additional runs performed with a Ford Falcon and a 13 tonne twin axle truck to represent a large car and a heavy commercial vehicle.

B.1.3 Results

Once the data had been gathered the vehicle simulation software was run and the lateral and vertical forces acting on the tyres obtained. Figures B.2 (a) to (c) show both the lateral and vertical forces acting on each of the tyres as simulated for the Nissan Pulsar, Ford Falcon and 13 tonne truck.

Figure B.2 Site 7A, vertical and lateral forces under each tyre at 62km/h for various vehicles

a) Nissan Pulsar

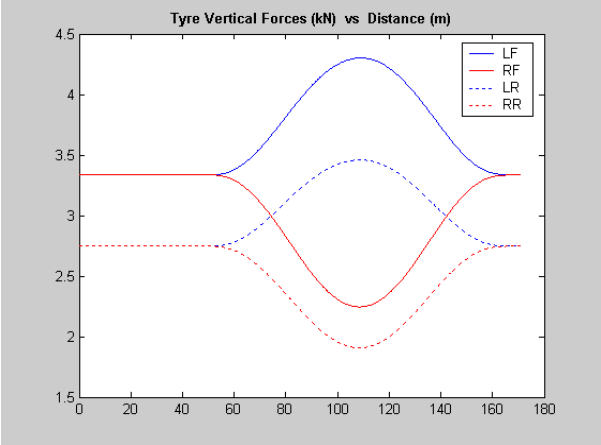

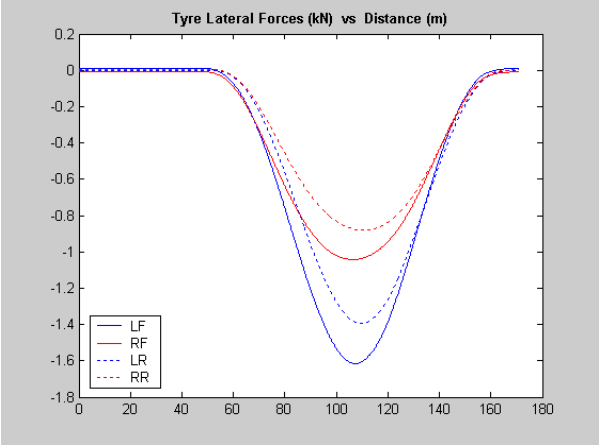

b) Ford Falcon

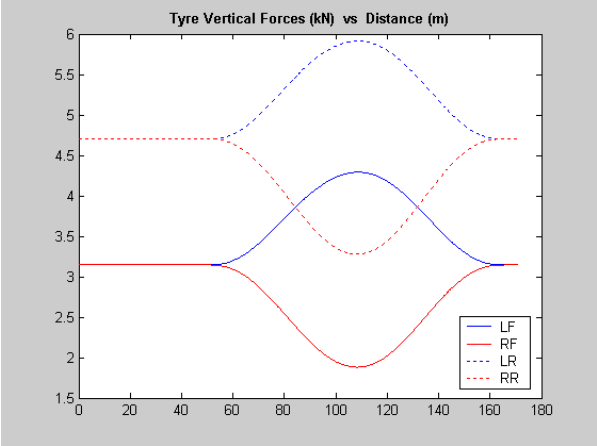

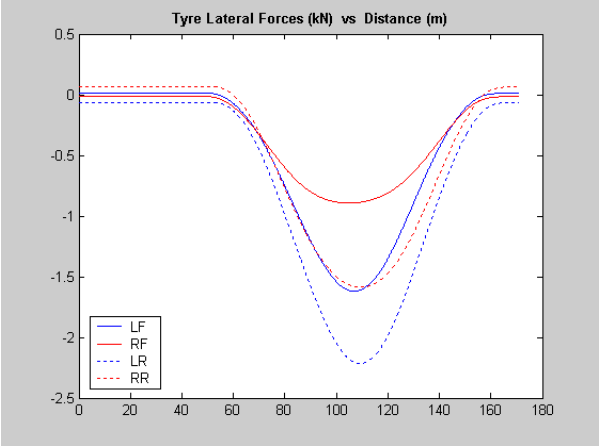

c) Truck

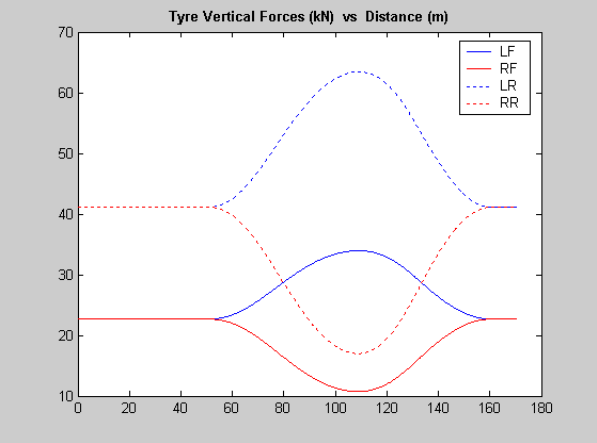

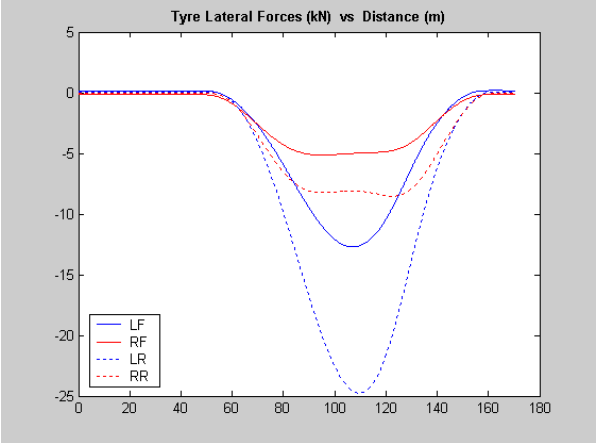

Note: LF=left front wheel, RF=right front wheel, LR=left rear wheel, RR=right rear wheel

As expected, both lateral and vertical tyre forces increased with increasing vehicle weight/size, the 13 tonne truck generating forces that were a factor of 10 greater than those generated by the passenger cars.

The peak lateral forces (PLFs) and the peak vertical forces (PVFs) were simulated using the Nissan Pulsar for each of the 23 sites and the results are shown in table B.2 below.

Table B.2 Simulated peak lateral and vertical forces using the Nissan Pulsar characteristics over each site

Site	Turn direction	Chip loss position (m)	Speed (km/h)	Peak lateral force (kN)				Peak vertical force (kN)			
				Left front	Right front	Left rear	Right rear	Left front	Right front	Left rear	Right rear
4	Left	127.4	76	0.894	1.250	0.765	1.109	2.45	4.13	2.07	3.34
4A	Right	none	78	-1.316	-0.924	-1.169	-0.791	4.16	2.41	3.36	2.03
7	Left	55.8	65	1.241	2.493	1.065	2.153	1.77	4.64	1.54	3.71
7A	Right	none	62	-1.615	-1.043	-1.393	-0.883	4.29	2.25	3.46	1.91
81	Left	94.7	63	1.334	3.770	1.169	3.148	1.32	5.01	1.18	3.96
81A	Right	none	62	-2.628	-1.261	-2.247	-1.083	4.69	1.72	3.74	1.50
82	Left	176.6	63	1.397	3.859	1.239	3.292	1.35	5.01	1.19	3.97
82A	Right	none	62	-2.629	-1.261	-2.247	-1.083	4.69	1.72	3.73	1.50
9	Left	79.8	80	1.048	1.661	0.913	1.493	2.19	4.32	1.87	3.48
9A	Right	none	79	-1.118	-0.868	-1.045	-0.735	3.86	2.50	3.32	2.11
10	Left	122.6	81	0.881	1.215	0.741	1.061	2.48	4.11	2.09	3.32
10A	Right	none	79	-1.059	-0.803	-0.931	-0.679	4.02	2.58	3.26	2.17
15	Left	47.9	25	0.729	1.507	0.757	0.997	2.55	4.13	2.08	3.30
16	Left	35.1	30	1.219	3.108	1.114	2.139	1.78	4.74	1.49	3.69
17	Left	56.7	68	1.063	1.680	0.901	1.460	2.20	4.33	1.88	3.49
17A	Right	none	67	-1.370	-0.949	-1.193	-0.803	4.18	2.38	3.37	2.02
18	Right	62.8	67	-3.215	-1.437	-2.953	-1.252	2.17	1.61	3.80	1.32
18A	Left	none	65	1.416	3.109	1.243	2.844	2.16	4.74	1.36	3.77
21	Right	61.1	69	-1.328	-0.932	-1.156	-0.787	4.16	2.41	3.37	2.04
21A	Left	none	70	1.137	1.917	0.964	1.666	2.08	4.43	1.77	3.56
22	Left	none	65	1.303	3.115	1.135	2.685	1.52	4.83	1.33	3.85
22A	Right	none	61	-1.876	-1.123	-1.622	-0.955	4.40	2.10	3.53	1.79
23	Left	38.5	28	1.050	2.477	1.012	1.668	2.10	4.52	1.69	3.55

B.1.4 Analysis of results

It was hypothesised that the displacement of the centre of the chip loss area would coincide with the location of the PLFs. To test this hypothesis the location of the average PLF for all four tyres from table B.2 was plotted against the displacement of the centre of the chip loss area. The resulting plot is shown in figure B.3.

Figure B.3 Position of the average peak lateral force for all four tyres against the location of the centre of the chip loss area

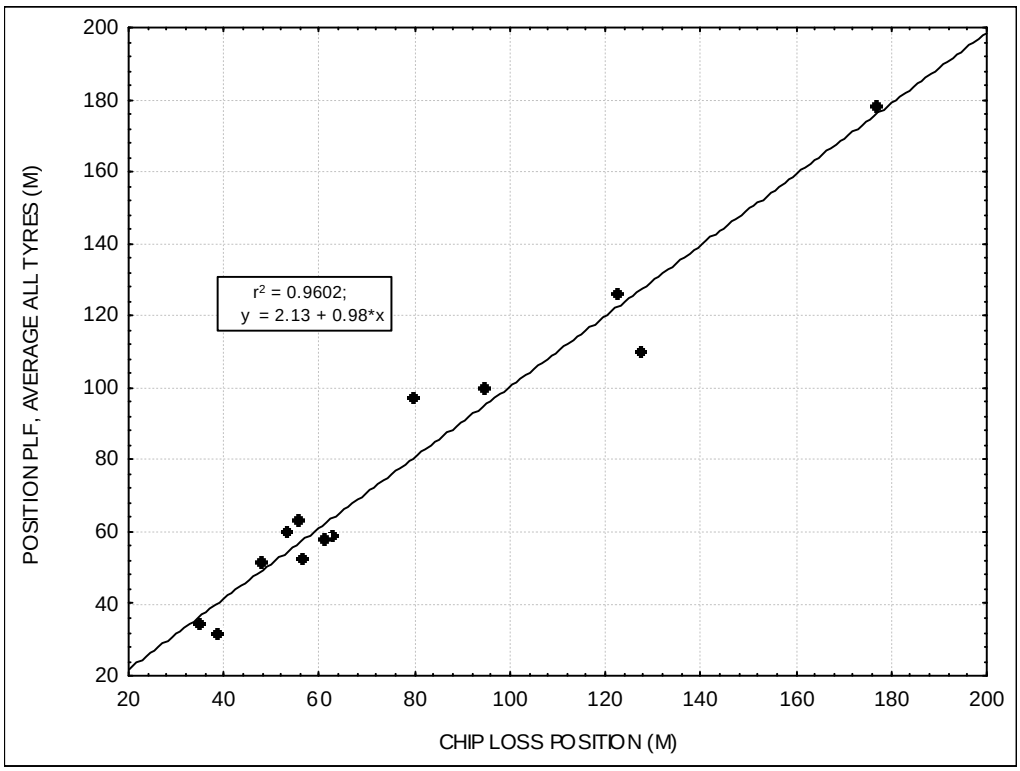

A linear regression was performed on the resulting curve and a correlation coefficient was found of r^2=0.9602. This result appears to confirm the hypothesis.

To aid the following discussion, the cornering terminology used is illustrated in figure B.4.

Figure B.4 Cornering terminology

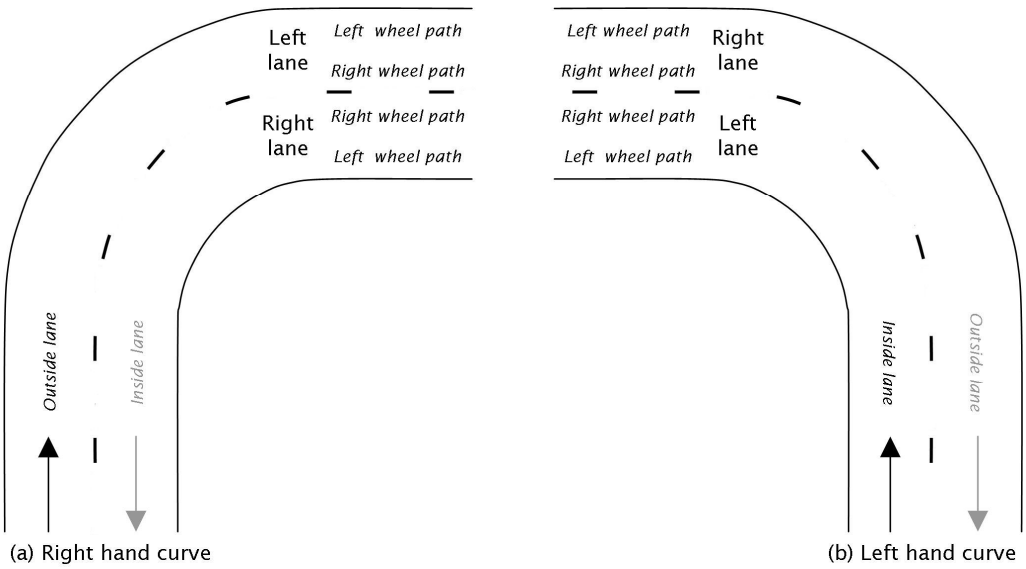

For left-hand curves, the PLFs for the left-hand lane are shown in figure B.5, for all four tyres. Similarly the PLFs in the right lane of left-hand curves are shown in figure B.6. Finally figure B.7 shows the PLFs in the left and right lanes of the two right-hand curves that showed chip loss.

Figures B.5 to B.7 show that the PLFs during cornering for front wheel drive vehicles like the Nissan Pulsar always occurred on the outside front wheel (ie right front wheel for a left-hand curve and left front wheel for a right-hand curve). Regarding maximum PLF, figures B.5 and B.6 show in the majority of cases this occurred in the inside (left) lane for left-hand curves. In contrast, no clear trend is evident in the results shown in figure B.7 for the two right-hand curves, with maximum PLF occurring in the inside (right) lane for site 21 and outside (left) lane for site 18.

For left-hand curves, except where chip loss had occurred across the whole width of the road due to a construction fault, chip loss was always observed in the inner wheel path of the left lane, ie under the left-hand wheels (see figure B.8). However, in all cases the highest lateral forces on left-hand curves were found to occur on the outer wheel path of the left lane (ie under the right-hand tyres). This is because body roll results in lifting the inside tyres and restricts the magnitude of the force that can be exerted before tyre slip occurs.

Few examples of chip loss on right-hand curves were found. In these cases, chip loss was again seen on the innermost wheel path (ie left wheel path of the right lane) despite larger magnitude lateral forces occurring on the outer (right) wheel path of the right lane.

Figure B.5 Peak lateral forces for left-hand curves with chip loss, left lanes

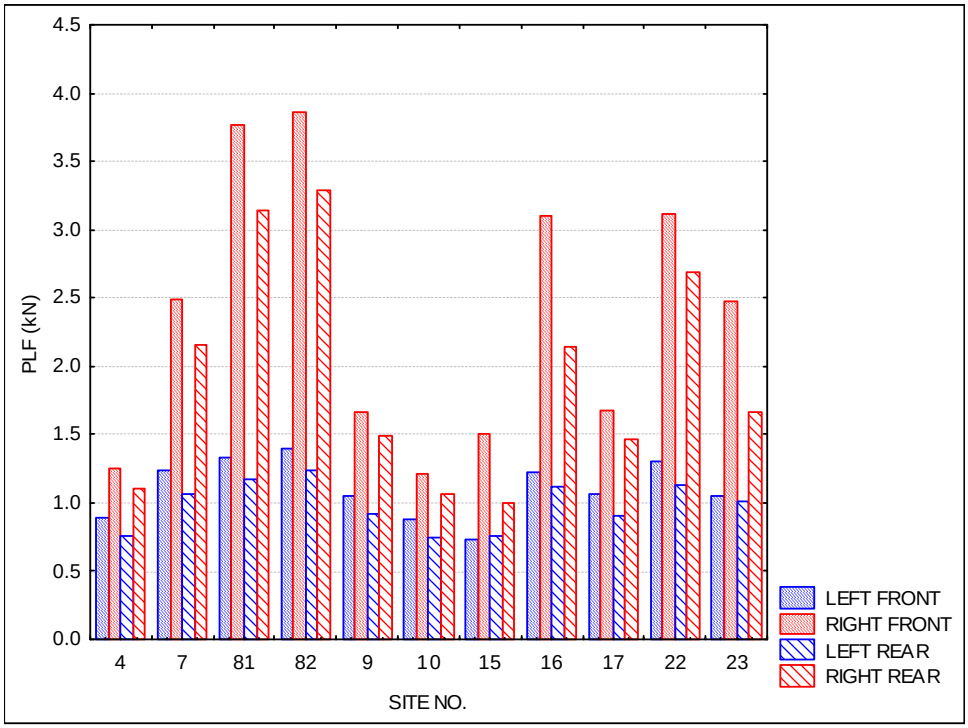

Figure B.6 Peak lateral forces for left-hand curves with chip loss, right lanes (right lanes had no chip loss)

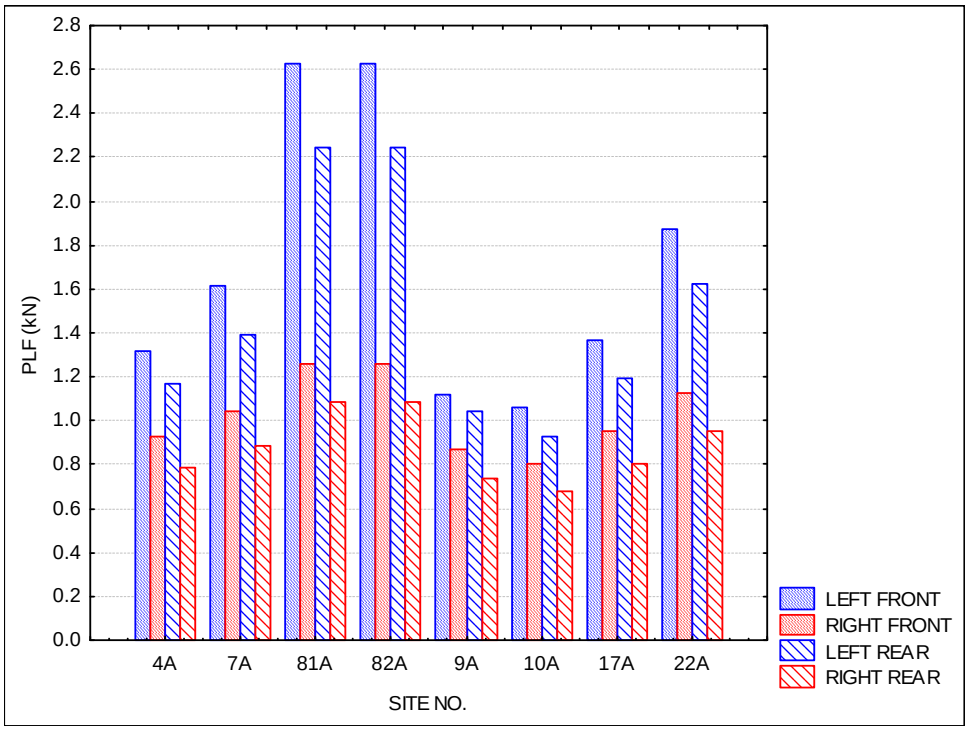

Figure B.7 Peak lateral forces in both the left and right lanes of right-hand curves (curves showed chip loss)

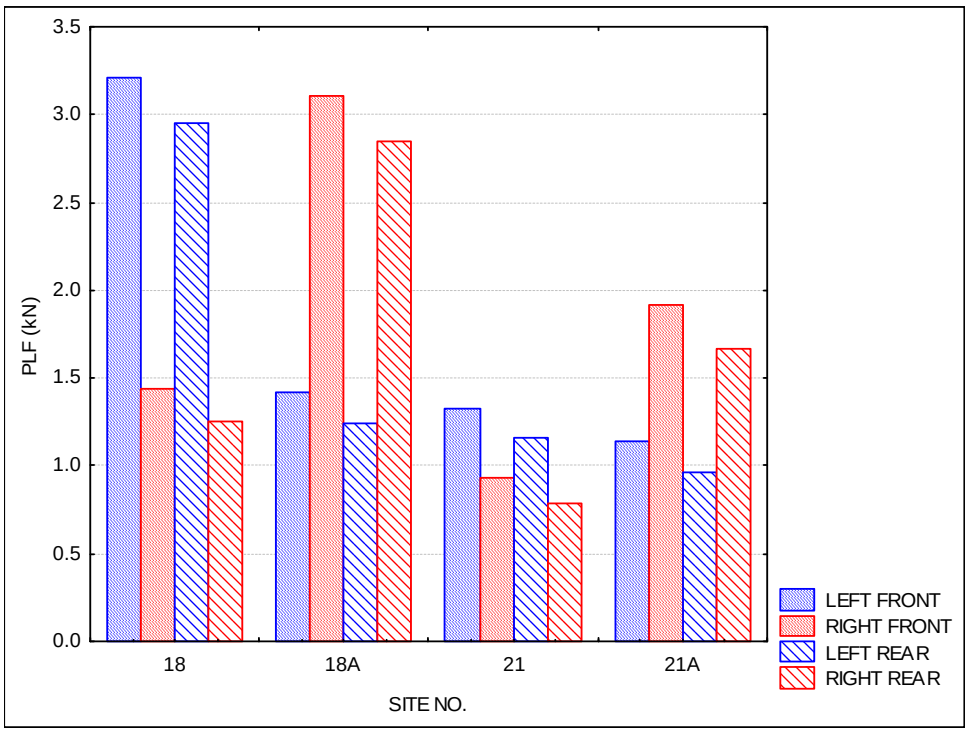

Figure B.8 Chip loss present on the inside wheel path of site 7

As stated earlier, for the sites studied, chip loss occurred on the inside wheel path. Although the measured PLFs were lower than those calculated for the outer wheel path, the PVFs were also lower as the weight of the vehicle moved to the outer tyres due to body roll. It seems plausible that the resulting tyre scrubbing action caused by the force distribution may be responsible for the observed chip loss.

To investigate this hypothesis a force ratio was calculated as follows:

Peak force ratio = peak lateral force/peak vertical force

The expectation was the greater the peak force ratio (PFR), the greater the likelihood of tyre scrubbing and therefore chip loss.

The PFR was calculated for each site by averaging the PLFs and the PVFs over each wheel path. Apart from one site, the PFR of the inside wheel path was shown to exceed that of the outer wheel path. Also, the maximum PFR was likely to occur in the inner-most wheel path of the curve.

For the left-hand curves, results for the left lane (chip loss lane) are shown in figure B.9 and for the right lane in figure B.10. As can be seen, the PFR of the inside wheel path exceeded that of the outer for both lanes apart from site 15, which was a 90º curve at an intersection of two suburban streets. The reason for its anomalous behaviour is unclear but possibly relates to the slow speed (25km/h) at which it was traversed resulting in little body roll.

Figures B.11 and B.12 compare the PFR of the wheel paths for left- and right-hand curves respectively. If scrubbing is a major mechanism for chip loss, then the PFR of the chip loss wheel path should be considerably higher than that of the equivalent path of the opposite lane. In other words, for left-hand curves, the PFR of left tyres for the left lane should be greater than the PFR of right tyres in the right lane. Conversely for right-hand curves, the PFR of the left tyres in the right lane should be greater than the right tyres in the left lane. This was generally observed apart from sites 4 and 18. Why these two sites did not conform to this theory is unclear but it is conjectured that absence of superelevation in the modelling could be the cause.

Figure B.9 Peak force ratio for left-hand curves with chip loss, left lanes

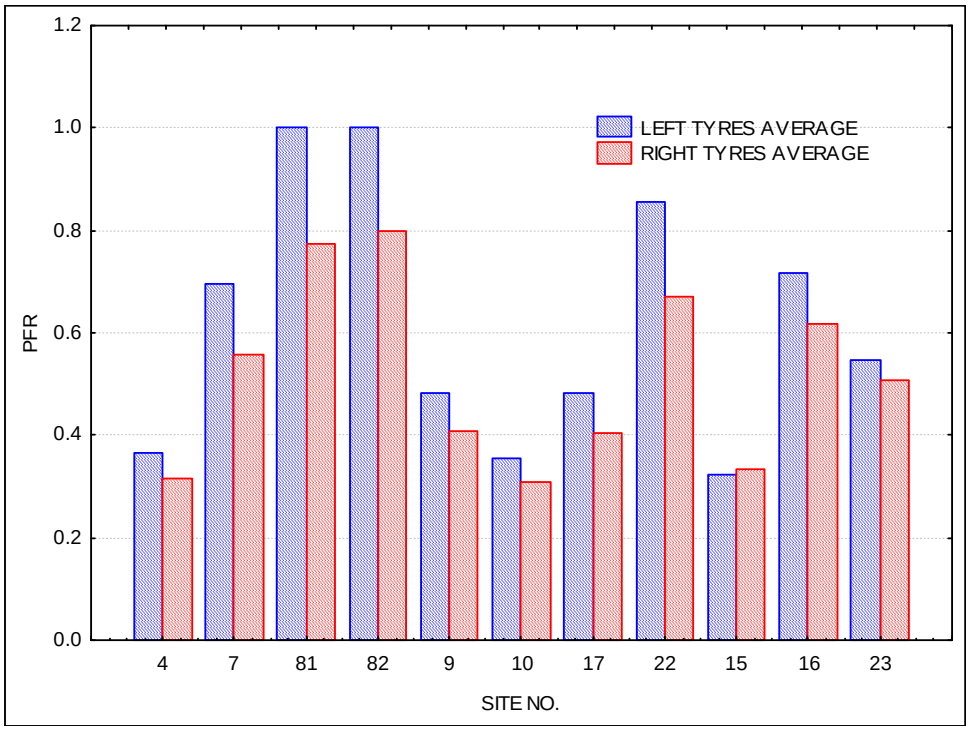

Figure B.10 Peak force ratio for left-hand curves with chip loss, right lanes (right lanes had no chip loss)

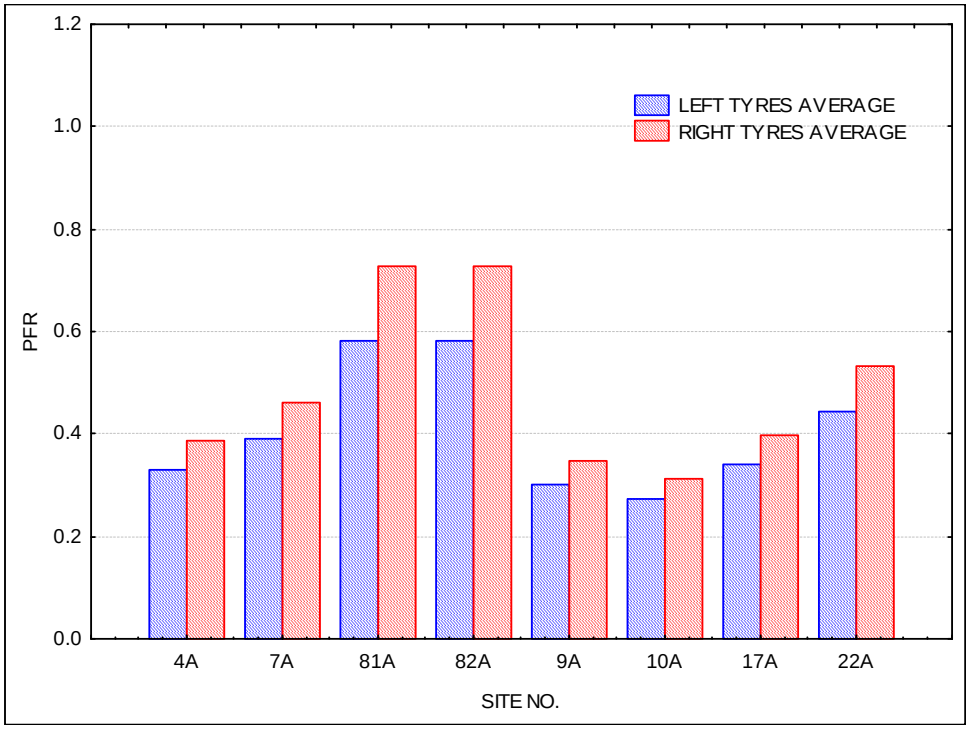

Figure B.11 Peak force ratio for left-hand curves, left and right lanes

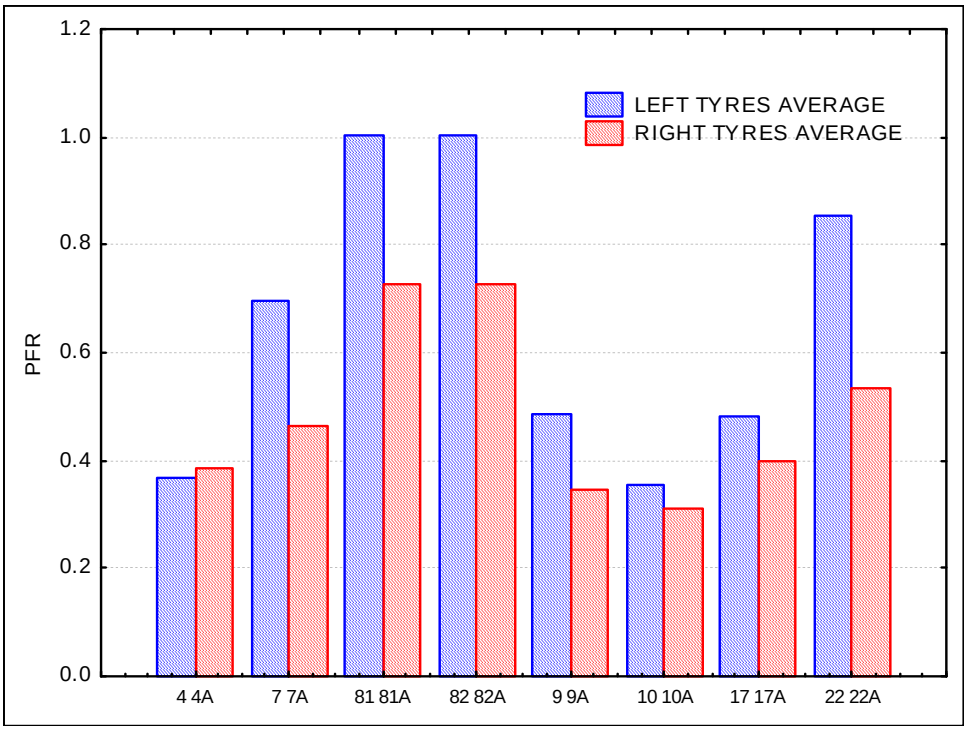

Figure B.12 Peak force ration for right-hand curves, left and right lanes

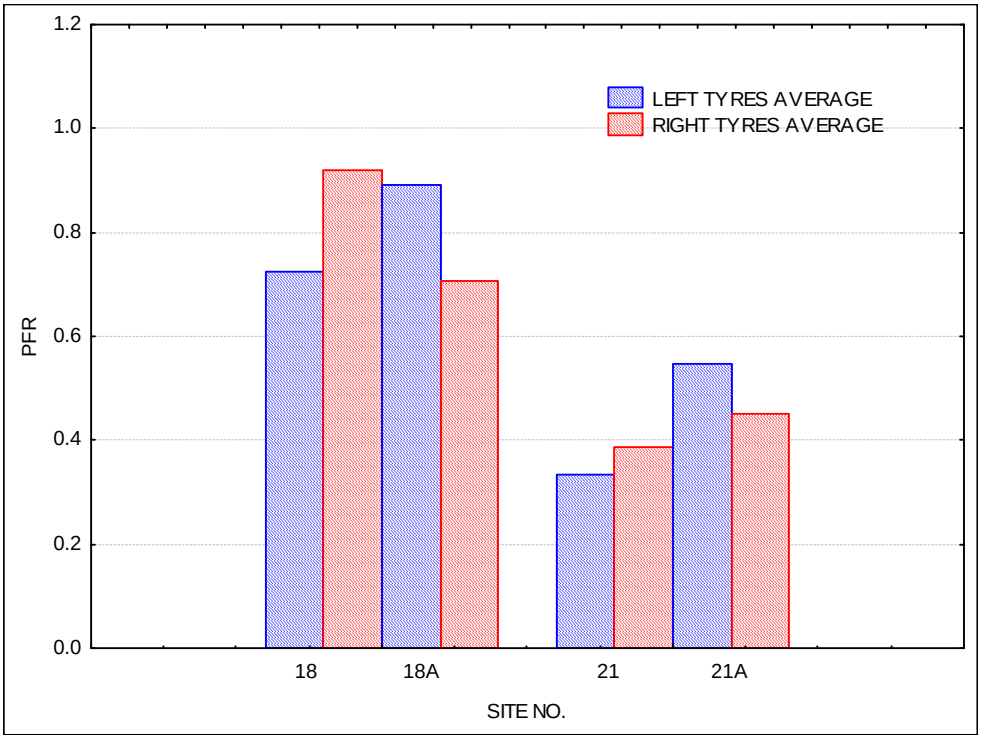

In general, for simple flat sites it can be expected chip loss will coincide with maximum PFR and so occur in the innermost wheel path of the curve, corresponding to the left wheel path of the left lane of left-hand curves and the left wheel path of the right lane of right-hand curves. This probably accounted for the rarity of sites exhibiting chip loss only in the outside lane of curves. Such loss could occur but only after or at the same time as chip loss occurred in the innermost wheel path. Whenever chip loss occurs in isolation in locations other than the innermost wheel path, it is likely to relate to seal texture variation. The tacit assumption made when comparing forces between wheel paths is that the surface across the road is uniform. However, for chipseal surfacings, bitumen application rates are typically based on an average value of the existing surface's texture depth. This may result, for example, in application rates being lower than desirable near the centre line and so the seal may be more susceptible to damage at this location.

With reference to figure B.13, it can be seen the longitudinal position of the PFR along a curve coincided with the longitudinal position of the PSF. This accounts for the similarity in the degree of correlation with chip loss position shown in figures 2.2 and B.3.

Figure B.13 Peak lateral force longitudinal position versus peak force ratio longitudinal position

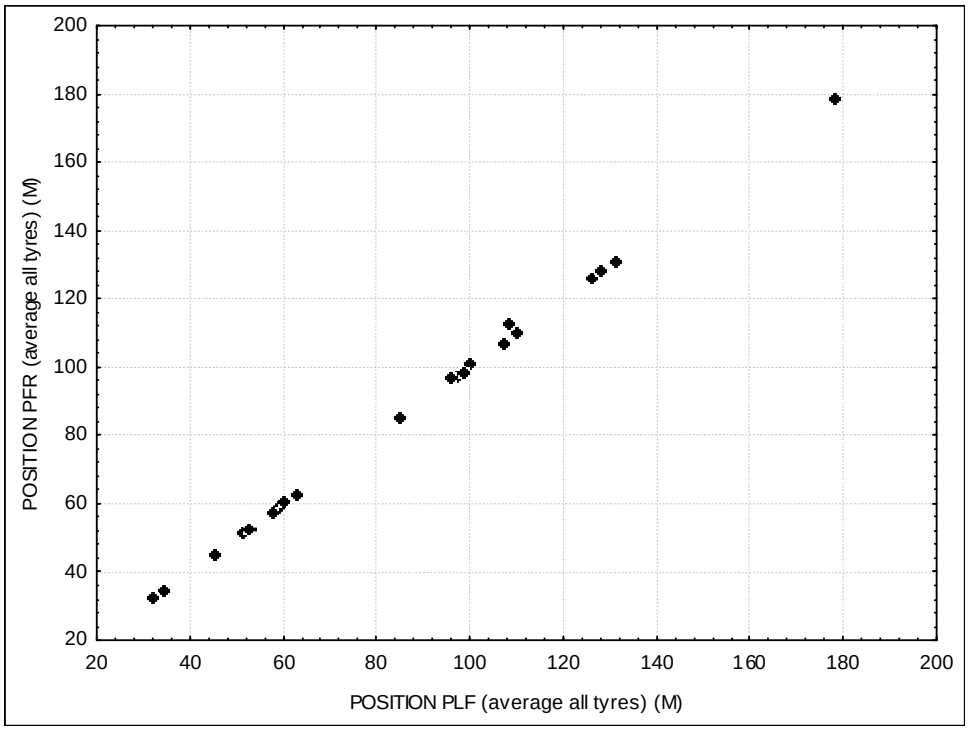

In summary, the results indicate that chip loss on curves was most likely to occur in the wheel path with the largest PFR and not simply the wheel path where the magnitude of the PLF was greatest. In nearly all cases the PFR occurred in the innermost wheel path of the curve.

Appendix C: Effects of road geometry and condition on cornering speeds

C.1 Data

The database of speed around curves produced by Koorey et al (2001) was divided into heavy and light vehicles for the purpose of analysis. It was anticipated heavy vehicles would travel at significantly lower speeds around the curves.

Speeds had been measured by the transit times between pairs of sensors placed around the curve. In most cases three sensors were used, but for two curves (both in increasing and decreasing directions) six sensors were used.

Because of variation in driving practice, there is no strongly consistent pattern of speed change from one sensor to another. The overall average trends obtained from examining the data for the corners with six sensors indicate speeds generally vary by a few km/h between sensors 2 and 5. If we take S_{i-i+1} as the speed indicated between the ith sensor and the next one around the curve we obtain the following best fit relationships:

$$S_{1\text{-}2} = 1.141\ S_{2\text{-}3} - 6.67 \qquad (r^2 = 0.867) \qquad \text{(Equation C.1)}$$

$$S_{3\text{-}4} = 1.028\ S_{2\text{-}3} - 3.78 \qquad (r^2 = 0.946) \qquad \text{(Equation C.2)}$$

$$S_{3\text{-}4} = 1.025\ S_{2\text{-}3} - 4.11 \qquad (r^2 = 0.946) \qquad \text{(Equation C.3)}$$

$$S_{5\text{-}6} = 0.938\ S_{2\text{-}3} - 1.67 \qquad (r^2 = 0.853) \qquad \text{(Equation C.4)}$$

Table C.1 gives comparative values calculated from the above equations for S_{2-3} equal to a low value of 40km/h and a high value of 120km/h.

Table C.1 Comparison of average speeds according to equations C1 to C4

$S_{1\text{-}2}$	$S_{2\text{-}3}$	$S_{3\text{-}4}$	$S_{4\text{-}5}$	$S_{5\text{-}6}$
39.0	40	37.3	36.9	35.8
130.2	120	119.6	118.9	110.9

In view of the relatively small variation of the speeds between sensors 2 and 5, it is satisfactory to take speed S_{2-3} as representative of the speeds around the curve. This allows us to use data from all the sites reported by Koorey et al (2001) in the following analysis.

C.2 Distribution of speeds

Tables C.2 and C.3 list statistical data for speeds S_{2-3} around the various curves investigated for both heavy and light vehicles respectively. In all cases it was possible to closely fit a normal curve to the data. The observed 5%, 85%, 95% and 99% levels of S_{2-3} are listed, along with the values calculated from the normal curve fits. Typically the standard deviation of speeds is of the order of 12% of the average speed. However, there are some cases with a higher spread of speeds resulting in a maximum standard deviation value of 23.6% (site 6 decreasing, heavy vehicles).

The means and standard deviations of speeds S_{2-3} for heavy vehicles are compared with those for light vehicles in table C.4. Although the average speed for light vehicles is always greater than that for the

heavier, the difference is usually only of the order of a few km/h. Exceptions are site 3, which is a tight hairpin curve, and site 9 in the decreasing direction. The ratio of the spread of speeds, as indicated in the ratio of standard deviations in the last column of table C.4, does not vary with the vehicle type in any systematic way.

Table C.2 Statistical analysis of speed $S_{2\text{-}3}$ data for all sites, heavy vehicles

Heavy vehicles		Mean	SD	SD/Mean	5%		85%		95%		99%	
Site	Dec/inc				Fit	Actual	Fit	Actual	Fit	Actual	Fit	Actual
3	I	36.26	4.45	0.123	28.9	27.1	40.9	40.0	43.6	42.3	46.6	45.3
3	D	39.12	6.49	0.166	28.4	28.9	45.8	45.7	49.8	49.7	54.2	56.9
4	I	42.67	7.86	0.184	29.7	27.1	50.8	48.8	55.6	53.7	61.0	64.9
4	D	42.45	6.93	0.163	31.1	31.3	49.6	48.1	53.8	52.3	58.6	70.0
5	I	52.61	9.27	0.176	37.4	41.9	62.2	59.1	67.9	62.2	74.2	89.5
5	D	56.02	6.54	0.117	45.3	45.2	62.8	62.6	66.8	67.4	71.2	76.0
6	D	69.19	16.36	0.236	42.3	40.5	86.1	84.2	96.1	89.0	107.2	92.0
7	I	81.10	9.98	0.123	64.7	66.4	91.4	90.2	97.5	100.5	104.3	106.6
7	D	79.74	10.02	0.126	63.3	66.2	90.1	89.3	96.2	96.6	103.0	108.3
9	I	90.21	9.89	0.110	73.9	73.4	100.5	99.7	106.5	106.0	113.2	114.8
9	D	81.62	9.88	0.121	65.4	66.6	91.9	90.0	97.9	96.3	104.6	105.7
11	I	83.11	9.66	0.116	67.2	69.6	93.1	92.6	99.0	98.9	105.6	103.0
11	D	82.38	10.88	0.132	64.5	64.2	93.7	92.6	100.3	101.0	107.7	107.3
12	I	53.94	6.91	0.128	42.6	39.0	61.1	60.0	65.3	65.3	70.0	67.3
12	D	57.92	7.47	0.129	45.6	47.2	65.7	63.9	70.2	69.5	75.3	78.1
13	I	45.72	7.72	0.169	33.0	29.8	53.7	52.2	58.4	59.3	63.7	63.3
13	D	50.27	5.72	0.114	40.9	42.0	56.2	54.6	59.7	59.0	63.6	71.0
16	I	79.89	9.27	0.116	64.6	65.1	89.5	87.8	95.1	93.5	101.5	107.2
16	D	78.36	9.16	0.117	63.3	62.8	87.9	87.9	93.4	92.2	99.7	100.9

Table C.3 Statistical analysis of speed $S_{2\text{-}3}$ data for all sites, light vehicles

Light vehicles		Mean	SD	SD/Mean	5%		85%		95%		99%	
Site	Dec/inc				Fit	Actual	Fit	Actual	Fit	Actual	Fit	Actual
3	I	38.92	4.61	0.119	31.3	32.2	43.7	43.9	46.5	45.3	49.7	51.6
3	D	43.41	5.13	0.118	35.0	33.7	48.7	48.7	51.8	51.3	55.3	55.5
4	I	43.54	6.01	0.138	33.7	33.7	49.8	48.8	53.4	53.7	57.5	57.2
4	D	43.66	5.63	0.129	34.4	34.7	49.5	49.7	52.9	52.3	56.8	56.5
5	I	53.56	7.71	0.144	40.9	42.5	61.5	60.2	66.2	64.9	71.5	77.0
5	D	58.98	7.12	0.121	47.3	48.3	66.4	64.9	70.7	71.4	75.5	79.4
6	D	70.51	12.34	0.175	50.2	48.9	83.3	82.3	90.8	87.6	99.2	98.6
7	I	81.96	10.11	0.123	65.3	66.4	92.4	92.6	98.6	100.5	105.5	106.6
7	D	80.67	10.08	0.125	64.1	63.8	91.1	89.3	97.3	96.6	104.1	105.1
9	I	91.89	10.09	0.110	75.3	73.9	102.3	101.6	108.5	108.4	115.4	117.5

Light vehicles		Mean	SD	SD/Mean	5%		85%		95%		99%	
Site	Dec/inc				Fit	Actual	Fit	Actual	Fit	Actual	Fit	Actual
9	D	89.56	12.13	0.135	69.6	70.2	102.1	103.4	109.5	108.0	117.8	117.6
11	I	85.78	9.48	0.111	70.2	71.2	95.6	95.5	101.4	101.1	107.8	108.3
11	D	85.27	10.49	0.123	68.0	67.1	96.1	96.5	102.5	101.8	109.7	109.0
12	I	55.35	6.16	0.111	45.2	43.7	61.7	61.7	65.5	64.0	69.7	70.2
12	D	59.05	7.24	0.123	47.1	49.4	66.6	66.6	71.0	71.9	75.9	78.1
13	I	47.67	6.44	0.135	37.1	38.2	54.3	53.9	58.3	58.1	62.6	62.9
13	D	52.67	6.31	0.120	42.3	43.6	59.2	58.5	63.1	63.6	67.4	72.2
16	I	80.29	9.69	0.121	64.3	65.1	90.3	88.9	96.2	95.9	102.8	107.2
16	D	79.04	9.05	0.115	64.2	64.4	88.4	87.9	93.9	92.2	100.1	100.9

Table C.4 Comparison of light and heavy vehicle speed data

Site	Direction Dec/inc	Mean speed diff Light – heavy (km/h)	Mean speed ratio Light/heavy	Ratio of speed standard deviations, light/heavy
3	I	2.7	1.074	1.037
3	D	4.3	1.110	0.790
4	I	0.9	1.020	0.764
4	D	1.2	1.028	0.813
5	I	0.9	1.018	0.832
5	D	3.0	1.053	1.088
6	D	1.3	1.019	0.754
7	I	0.9	1.011	1.013
7	D	0.9	1.012	1.006
9	I	1.7	1.019	1.021
9	D	7.9	1.097	1.228
11	I	2.7	1.032	0.982
11	D	2.9	1.035	0.963
12	I	1.4	1.026	0.892
12	D	1.1	1.020	0.969
13	I	2.0	1.043	0.833
13	D	2.4	1.048	1.103
16	I	0.4	1.005	1.045
16	D	0.7	1.009	0.989

C.3 Influence of lane roughness

Values for a number of properties which might be expected to affect vehicle speed around curves were available, namely:

- The average daily traffic (ADT). Density of traffic might be expected to affect driving behaviour.

- The deflection angle, ie the change in direction over the curve length.
- The average gradient over the curve length.
- The minimum advisory speed, calculated as the theoretical advisory speed for the minimum radius encountered on the curve (refer equation 3.1). This provides an estimate of the safe curve speed.
- The average speed environment (ASE) calculated as the mean of the theoretical advisory speed through the curve. This is used as an estimate of the approach speed estimate.
- The average roughness (AR) throughout the curve. Roughness figures corresponding to the time of the speed measurement trials were in NAASRA counts. The AR values used in the regression analysis ranged from a minimum of 42 NAASRA counts/km to a maximum of 117 NAASRA counts/km.

Forward regressions of mean speed (S_{2-3}), and 5%, 85%, 95% and 99% levels estimated from the normal curve fits were carried out against all the above variables, for both heavy and light vehicle classes. In all cases the only significant factors affecting vehicle speed parameter were the ASE and the AR. Gradient, in particular, unexpectedly had a negligible effect. Square root values and squares of ASE and AR were compared to the original values, and were found to be insignificant.

The general speed relationship thus takes the form:

$$S_{2\text{-}3}\,(V,p) = a_0 + a_1\,ASE - a_2\,AR \qquad \text{(Equation C.5)}$$

V is the vehicle type (heavy or light), and p the percentage level (=50% for the mean speed). The speed parameter increases as ASE increases and decreases with increasing roughness. Table C.5 summarises the results, along with the goodness of fit data (r^2 and standard error (SE) of the predicted quantity).

Table C.5 Parameters for equation C5

V	p	a_0	a_1	a_2	r^2	SE
Heavy	5%	0.21	0.6951	0.1481	0.8756	5.5
Light	5%	10.95	0.6294	0.174	0.8926	4.9
Heavy	50%	15.67	0.7522	0.2233	0.8861	6.1
Light	50%	21.82	0.7339	0.2532	0.895	5.9
Heavy	85%	25.41	0.7881	0.2708	0.8621	7.4
Light	85%	28.67	0.7996	0.3031	0.8897	6.8
Heavy	95%	31.13	0.8092	0.2986	0.8429	8.3
Light	95%	32.69	0.8283	0.3324	0.8849	7.4
Heavy	99%	37.54	0.8328	0.3298	0.8195	9.5
Light	99%	37.19	0.8815	0.3652	0.8791	8.1

A more detailed analysis of the form of each curve (ie horizontal and vertical curvature) and the general environment may provide more accurate estimates of the speed profiles of curves, but it is clear the ASE and surface roughness values are by far the dominant factors determining the speed of cornering traffic.

C.4 Site locations

These are as indicated in table C.5 and covered horizontal curve radii from 27m to 215m.

Table C.5 Location of curves used to derive cornering speed relationships

Site	Dec/inc	Start location	Minimum radius of curvature (m)
3	I	SH2 RP 921/4.92	30
3	D	SH2 RP 921/5.02	27
4	I	SH2 RP 931/3.96	29
4	D	SH2 RP 931/3.96	29
5	I	SH2 RP 931/9.03	50
5	D	SH2 RP 931/9.06	49
6	D	SH2 RP 921/3.05	107
7	I	SH 53 RP 0/14.73	117
7	D	SH 53 RP 0/14.80	116
9	I	SH 2 RP 858/8.06	151
9	D	SH 2 RP 858/8.16	151
11	I	SH 3 RP 491/5.37	215
11	D	SH 3 RP 491/5.51	187
12	I	SH 2 RP 931/8.29	63
12	D	SH 2 RP 931/8.30	66
13	I	SH 2 RP 931/2.57	44
13	D	SH 2 RP 931/2.67	44
16	I	SH 57 RP 26/2.71	143
16	D	SH 57 RP 26/2.90	137

Appendix D: Glossary

2D	two-dimensional
ABAQUS	a finite element analysis package
ADT	average daily traffic
AR	average roughness
AS	curve advisory speed ≡ 85 percentile curve speed
AS_BND	curve advisory speed banded
ASE	average speed environment
CHCV	cumulative HCV passes, the product of the HCV passes and seal age
CHCVL	cumulative HCV loading, the product of the HCVL and seal age
CHCVL_BND	cumulative HCV loading banded
CLCV	cumulative LCV passes, the product of the LCV passes and seal age
CLCV_BND	cumulative LCV passes banded
CS	cornering or curve speed (km/h)
ECF_BND	estimated cornering force banded
ESA	equivalent standard axle
FE	finite element
FEA	finite element analysis
FORTRAN	the IBM Mathematical **For**mula **Tran**slating System
g	acceleration due to gravity (9.81 m/s^2)
HCV	heavy commercial vehicle
HCVL	the product of HCV and loading 'esa_vehicle'
HCV_BND	heavy commercial vehicle banded
HCVL_BND	the product of HCV and loading 'esa_vehicle' banded
HV	the proportion of heavy vehicles
LA	lateral acceleration (m/s^2)
LCV	light commercial vehicle
loading_esa_vehicle	equivalent standard axle loading for each vehicle type
LV	the proportion of light vehicles
LWP	left wheel path
MSSC	mean summer SCRIM coefficient
NAASRA	National Association of Australian State Road Authorities
NZTA	New Zealand Transport Agency (the crown entity responsible for New Zealand's SH network)
PFR	peak force ratio
PLF	peak lateral force
PLFHV	the simulated maximum peak lateral force of the inner wheel path of heavy vehicles
PLFLV	the simulated maximum peak lateral force of the inner wheel path of light vehicles
PSV	polished stone value (BS 812, part 114: 1989)
PVF	peak vertical force
RAMM	road assessment and maintenance management system

RWP	right wheel path
SCRIM	sideways force coefficient routine inspection machine (the skid tester employed in annual high-speed data surveys commissioned by NZTA on New Zealand's SH network.)
SCRIM RV	SCRIM reporting value which is the equilibrium SCRIM coefficient (ESC) value minus the T10 investigatory level (IL) for the particular skid site category
SD	standard deviation
SE	standard error
SH	state highway
T10:2010	The NZ Transport Agency document 'Specification for state highway skid resistance management'
TNZ P/17	The Transit NZ 2002 document 'Performance based specification for reseals. TNZ P/17:2002